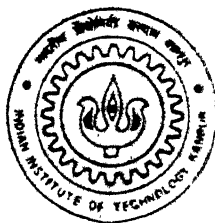


# ONE DIMENSIONAL TRANSIENT SIMULATION OF $pn$ JUNCTION DIODES

by

**Pratul Sharma**



TH  
/1999/M  
5230

Department of Electrical Engineering

**INDIAN INSTITUTE OF TECHNOLOGY KANPUR**

March, 1999

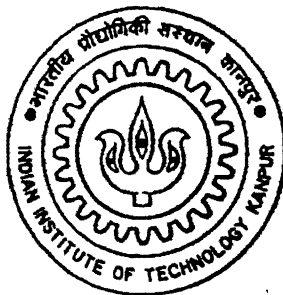
# ONE DIMENSIONAL TRANSIENT SIMULATION OF $pn$ JUNCTION DIODES

*A Thesis submitted  
in Partial Fulfillment of the Requirements  
for the degree of*

**Master of Technology**

*by*

**Pratul Sharma**



to the

**DEPARTMENT OF ELECTRICAL ENGINEERING  
INDIAN INSTITUTE OF TECHNOLOGY, KANPUR**

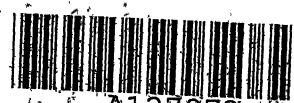
*March 1999*

20 MAY 1999 JEE

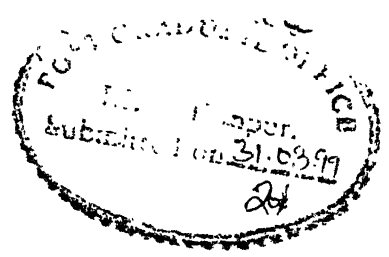
CENTRAL LIBRARY  
I. I. T., KANPUR

TH  
EE/1999/1-2  
Sh 282

Acc. No. A 127973



A127973



# Certificate

This is to certify that the work contained in the thesis entitled “**One dimensional transient simulation of  $pn$  junction diodes**” by **Pratul Sharma** has been carried out under my supervision and that this work has not been submitted elsewhere for the award of a degree.

*M.B. Patil*

**(Dr. M.B Patil)**

Assistant Professor

Department of Electrical Engineering,  
Indian Institute of Technology, Kanpur

March 1999.

# Acknowledgements

I sincerely thank Dr. M.B Patil for his valuable guidance and co-operation throughout the programme. His invaluable words have always inspired me to work properly and consistently.

I express my sincere regards to my teachers Dr Aloke Dutta, Dr. S. Kar and Dr. Subir Roy whose courses have raised my knowledge-level. I would also like to thank Dr B. Mazahari for his suggestions during my thesis work.

I would also thank Mr. Shafi for his help in the lab whenever I required. Finally, a special thanks to my friends Ravi, Jay, Pawan, Ritesh, Sandhitshu, Arindamb, Ashok(ji), Abhirup(da), Gautam(da), Atnu(da), S. Ganguly, Arvind and Karthik who made my stay at IIT Kanpur, a pleasurable and enjoyable one.

**Pratul Sharma**

# Abstract

A numerical simulation of diode using finite difference method is carried out for the turn ON and turn OFF transient conditions. The method is applicable to long-base and short-base diode for any type of doping profile. For a specified input waveform of current or voltage as a function of time, the program yields terminal currents and various quantities of interest in the interior of the device such as minority carrier density, different current components, electric field, electrostatic potential etc, as a function of time and position. The effect of changing external voltage, load resistance and the lifetime of the carriers on the turn OFF transient is investigated and comparison with analytical results is made. The comparison between simulated and SPICE results for the turn OFF transient is also presented.

# Contents

List of Figures	v
List of Tables	ix
<b>1 Introduction</b>	<b>1</b>
<b>2 Basic semiconductor Equations and Device Simulation</b>	<b>4</b>
2.1 Basic semiconductor equations . . . . .	4
2.2 Scaling . . . . .	6
2.3 Discretization of basic semiconductor equations . . . . .	7
2.4 Discretized equation for the transient condition . . . . .	10
2.5 Boundary conditions . . . . .	11
<b>3 Results and discussion</b>	<b>15</b>

3.1	Turn on transient . . . . .	16
3.1.1	Small current step . . . . .	16
3.1.2	High current step . . . . .	22
3.1.3	Voltage step . . . . .	26
3.2	Turn off transient . . . . .	29
3.3	Comparison with SPICE . . . . .	32
4	<b>Conclusion and scope for future work</b>	<b>41</b>
	<b>References</b>	<b>43</b>

# List of Figures

2.1	Discretization scheme . . . . .	8
2.2	Finite difference scheme . . . . .	9
2.3	Change in $\psi$ , $n$ and $p$ with time . . . . .	11
2.4	Energy band diagram for $pn$ diode: (a) at equilibrium. (b) when external voltage is applied. . . . .	12
2.5	Different types of excitations. . . . .	13
3.1	Sample . . . . .	15
3.2	Turn ON step. . . . .	16
3.3	Variation of diode voltage with time for small current step. . . .	17
3.4	Displacement current density vs distance for small current step.	18
3.5	Electron current density vs distance for small current step. . . .	18
3.6	Hole current density vs distance for small current step. . . . .	19

3.7	Minority carrier (electrons on $p$ side) concentration vs distance for small current step. . . . .	19
3.8	Electric field (at $x= 300.0022 \mu m$ ) vs time for small current step.	20
3.9	Electric Field vs distance for small current step. . . . .	20
3.10	Electrostatic potential vs distance for small current step. . . . .	21
3.11	Diode voltage vs time for high current step. . . . .	23
3.12	Displacement current density vs distance for high current step in the transition region. . . . .	23
3.13	Displacement current density vs distance for high current step in the neutral region . . . . .	24
3.14	Electron current density vs distance for high current step. . . . .	24
3.15	Hole current density vs distance for high current step. . . . .	25
3.16	Minority carrier (electrons on $p$ side) concentration vs distance for high current step. . . . .	25
3.17	Electrostatic potential vs distance for high current step. . . . .	26
3.18	Variation of diode current vs time for voltage step. . . . .	27
3.19	Displacement current density vs distance for voltage step. . . . .	28
3.20	Electrostatic potential vs distance for voltage step. . . . .	28

3.21	Minority carrier concentration (electrons on $p$ side) vs distance for voltage step. . . . .	29
3.22	(a) Input Voltage vs time; (b) Diode Voltage vs time; (c) Diode Current vs time; (d) Electric field near the junction vs time. . .	33
3.23	Turn off transient of the diode current vs time for different ex- ternal load, keeping the forward and the reverse bias constant. .	34
3.24	Turn off transient of the diode current vs time for different re- verse biases, keeping the forward bias constant. . . . .	34
3.25	Storage time delay vs Reverse bias. . . . .	35
3.26	Fall time delay vs Reverse bias. . . . .	35
3.27	Turn off transient of the diode current vs time for different for- ward biases, keeping the reverse bias constant. . . . .	36
3.28	Storage delay time vs Forward bias. . . . .	36
3.29	Fall time delay vs Forward bias. . . . .	37
3.30	Minority carriers concentration vs distance for different values of $\tau_n$ and $\tau_p$ . . . . .	38
3.31	Storage time delay vs $\tau_n/\tau_p$ . . . . .	39
3.32	Fall time delay vs $\tau_n/\tau_p$ . . . . .	39
3.33	Diode current vs time. . . . .	40

3.34 Minority carrier concentration vs distance for a short base diode  
after the negative edge of the voltage step. . . . . 40

# List of Tables

2.1   Scaling factors . . . . . 7

# Chapter 1

## Introduction

Most of the semiconductor devices contain at least one junction between p-type and n-type semiconductor materials.  $pn$  junctions are fundamental to the performance of many electronic circuits. The  $pn$  junction diode is a two terminal device which can perform various functions: (i) it is capable of rectifying low frequency alternating signals, (ii) because of non ohmic nature of the I-V curve a  $pn$  diode can be used as a variable resistor (varistor), (iii) since the depletion layer capacitance of such  $pn$  junction can be made to vary as some suitable function of reverse bias applied to them, the diodes have been used as a variable capacitors (varactors), (iv) due to non linear nature of I-V characteristic,  $pn$  junction diodes are used in demodulation of communication signals, (v) if the terminals of such junction are left open and the junction is irradiated externally, carriers are generated, and according to their polarity they are collected by appropriate ends of the depletion layer, this causes an open circuit voltage to develop across the  $pn$  junction. Hence they can be used as solar cells, (vi) direct bandgap semiconductors can be used as LEDs and

semiconductor lasers.

An important feature of a semiconductor diode is the similarity of its I-V characteristics with an ideal switch, hence, diodes are very important element in pulse electronics (mainly as a switching element in computers). High speed pulse diodes are also very important in radar and other branches of high and super-high frequency electronics. The rapid advancement in computer technology led to the development of new construction principle of logic, memory and other computer elements, which call for switching of large current. It therefore becomes necessary to create high speed diodes capable of switching on currents in a very short period of time. Hence, pulsed diodes with high frequency and power are required.

The development of new semiconductor technologies and novel semiconductor device structures has traditionally been guided by experimental approaches. Starting from an established process sequence, fabrication steps are changed together with geometrical dimensions (feature size). The modified process is then realized by fabricating several lots. The finished devices are tested to ensure that their performance conforms to the initial design specifications. This approach usually includes several iterations of the process to testing loop. With the advent of increasingly complex integrated circuits, the traditional empirical approach becomes expensive and time consuming.

In order to characterize the devices in a reasonable way, *numerical methods* emerge out to be an excellent solution. In the numerical methods, the actual device behaviour is simulated, taking into account semiconductor physics in detail. This is, of course, an intensive procedure in terms of the CPU time. However, it yields very useful information.

Numerical simulation of a semiconductor device is carried out by solving three non-linear partial differential equations, i.e. Poission's equation and two continuity equations, one for electrons and the other for holes, inside the geometry of the device. Modelling based on partial differential equations, which describe different regions of semiconductor devices in a unified manner was suggested by Gummel[1] for the one dimensional bipolar transistor. This approach was further developed and applied to  $pn$  junctions by De Mari[2], and to IMPATT diode by Scharfetter and Gummel [3].

The present thesis work deals with the simulation of a one dimensional silicon  $pn$  junction diode for the switching conditions. In Chapter 2, basic semiconductor equations, their discretization and the boundary conditions for the different types of excitations are described. The results obtained from the simulation and the analytical expressions are described in Chapter 3. In the last chapter (Chapter 4) conclusion and scope for future work are given.

# Chapter 2

## Basic semiconductor Equations and Device Simulation

### 2.1 Basic semiconductor equations

To determine the behavior of an arbitrary semiconductor structure under various operating conditions, a mathematical model is required. The semiconductor devices operate under non-equilibrium conditions in which electron and hole current flow through the device. The carrier current at any point in the device can be calculated by the electric field and the carrier concentration gradient at that point. Hence, to calculate the quantities of interest we require appropriate mathematical expressions.

The basic semiconductor equations are used to describe the static and dynamic behavior of carriers in the semiconductor under the influence of external fields which causes the deviation from the thermal equilibrium conditions. The

three basic semiconductor equations [4] are given as:

1. Poisson's equation

$$\nabla^2 \psi = -\frac{\rho}{\epsilon}, \quad (2.1)$$

where,  $\psi$  = electrostatic potential,  $\rho$  = space charge density =  $q(p - n + N_d^+ - N_a^-)$ ,  $N_d^+$  = ionized donor density,  $N_a^-$  = ionized acceptor density.

The Poisson's equation relates the potential to the charge density and thus enables us to determine the electric field for a given charge distribution.

2. Continuity equation for electrons

$$\nabla \cdot (D_n \nabla n - \mu_n n \nabla \psi) - R(n, p) = \partial n / \partial t \quad (2.2)$$

3. Continuity equation for holes

$$\nabla \cdot (D_p \nabla p + \mu_p p \nabla \psi) - R(n, p) = \partial p / \partial t \quad (2.3)$$

where  $D_n$  = diffusion constant for electron,  $D_p$  = diffusion constant for holes,  $R$  = recombination rate which is given by the Shockley-Read-Hall formula

$$R = \frac{np - n_i^2}{\tau_{n0}(p + p_t) + \tau_{p0}(n + n_t)} \quad (2.4)$$

where  $n_t$  = electron trap density,  $p_t$  = hole trap density,  $\tau_{n0}$  = electron lifetime,  $\tau_{p0}$  = hole lifetime.

The continuity equation expresses the principle of particle conservation by relating the net rate of change of charge carriers in a volume to the process that introduce and remove the carriers.

The Poisson's Equation is elliptic and the continuity equation is parabolic in nature. To analyze the behaviour of the device, above system of partial

differential equations is to be solved, however, in general, these equations cannot be solved analytically. Hence numerical methods are used to solve these equations. There are three tasks involved to solve these equations which are as follows:

1. The domain, i.e., the simulation geometry of the device is divided into finite number of partitions (grid points), where the solution can be approximated with the desired accuracy.

2. The differential equations are approximated in each of the domain by algebraic equations which involve only values of the continuous dependent variables at discrete points in the domain, and the knowledge of the structure of the chosen function which approximate the dependent variables within each of the sub domain. Hence, a large number of nonlinear algebraic equations are obtained with unknowns comprised of approximations of continuous dependent variables at discrete points.

3. The system of nonlinear equations is solved using the Newton Raphson method.

## 2.2 Scaling

The first step before the analysis of the semiconductor equations is proper scaling because the dependent variables ( $\psi, n, p$ ) in the basic semiconductor equations have large difference in magnitude. After scaling all the variables involved in the semiconductor equations have nearly same range of variation. In the present work the scaling factors used are given in Table 2.1.

quantity	symbol	value
$x$	$x_0$	$\max( x )$
$\psi$	$\psi_0$	$kT/q$
$n, p, C$	$C_0$	$\max C(x) $
$D_n, D_p$	$D_0$	$\max(D_n, D_p)$
$R$	$R_0$	$D_0 C_0 / x_0^2$
$t$	$t_0$	$x_0^2 / D_0$

Table 2.1: Scaling factors

After scaling the basic semiconductor equations becomes:

$$\lambda^2 \nabla^2 \tilde{\psi} - (\tilde{n} - \tilde{p} - \tilde{C}) = 0 \quad (2.5)$$

$$\nabla \cdot (\tilde{D}_n \nabla \tilde{n} - \mu_n \tilde{n} \nabla \tilde{\psi}) - \tilde{R}(n, p) = \frac{\partial \tilde{n}}{\partial t} \quad (2.6)$$

$$\nabla \cdot (\tilde{D}_p \nabla \tilde{p} + \mu_p \tilde{p} \nabla \tilde{\psi}) - \tilde{R}(n, p) = \frac{\partial \tilde{p}}{\partial t} \quad (2.7)$$

## 2.3 Discretization of basic semiconductor equations

There are several methods of deriving algebraic equations from the differential equations. In the present work, we are using the finite difference method. The whole analysis is carried out in one dimension.

In the finite difference method, the domain in which the solution is to be obtained is partitioned into subregions. In one dimensional case, the boundary of the domain is two points A and B, as shown in the Fig 2.1 . Between A and

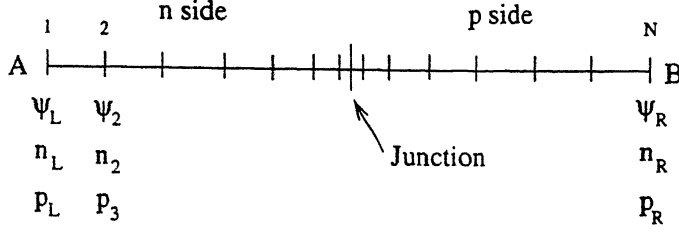


Figure 2.1: Discretization scheme

B is the interior of the device, where the solution is required. At each node the values of the unknowns are represented by  $\psi_i$ ,  $n_i$ ,  $p_i$ . For each node we have three unknowns and three equations and also at the boundary, we have appropriate boundary conditions for each unknown. Hence for  $N$  nodes we will get  $3N$  equations.

First we will derive the difference equations for the static semiconductor equations, which are obtained if the boundary conditions for the electrostatic potential are time invariant. The partial derivatives of electron and hole concentration with respect to time vanish in this case. Hence the basic semiconductor equations becomes:

$$\lambda^2 \cdot \nabla^2 \tilde{\psi} - (\tilde{n} - \tilde{p} - \tilde{C}) = 0 \quad (2.8)$$

$$\nabla \cdot (\tilde{D}_n \nabla \tilde{n} - \mu_n \tilde{n} \nabla \tilde{\psi}) - \tilde{R}(n, p) = 0 \quad (2.9)$$

$$\nabla \cdot (\tilde{D}_p \nabla \tilde{p} + \mu_p \tilde{p} \nabla \tilde{\psi}) - \tilde{R}(n, p) = 0 \quad (2.10)$$

To derive the difference equations, the differential operators are directly replaced by the difference operators. For the Poisson's equation, it is assumed that the electrostatic potential varies linearly between two adjacent points, as shown in Fig 2.2. Thus we can write

$$\frac{\partial \psi}{\partial x} \Big|_i = \frac{\psi_{i+1/2} - \psi_{i-1/2}}{\frac{h_i + h_{i-1}}{2}} \quad (2.11)$$

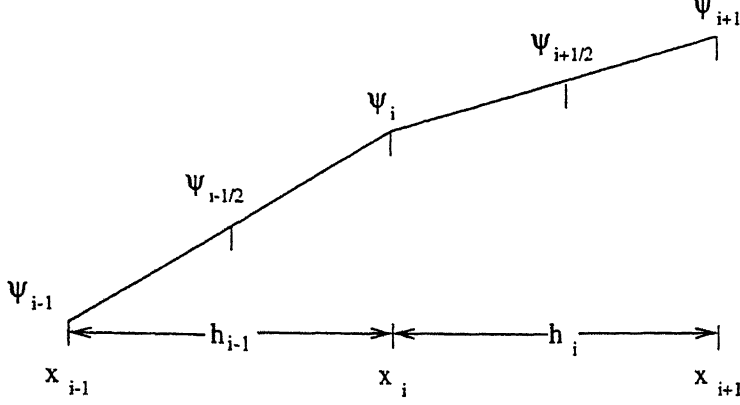


Figure 2.2: Finite difference scheme

$$\frac{\partial^2 \psi}{\partial x^2} \Big|_i = \frac{d\psi/dx \Big|_{i+1/2} - d\psi/dx \Big|_{i-1/2}}{\frac{h_i + h_{i-1}}{2}} \quad (2.12)$$

For continuity equations, the assumption of  $n$  and  $p$  varying linearly between two grid points is not valid, because the percentage variation of  $n$  and  $p$  between the two grid points is much more than that of the electrostatic potential  $\psi$ . Hence, the discretization of the continuity equation is carried out using the Scharfetter and Gummel approximation [3]. In this approximation, it is assumed that the variation of  $n$  and  $p$  between two adjacent grid points is exponential in nature. The discretized continuity equation for electrons is given by [4]

$$D_n \left[ \frac{B(\psi_{i+1} - \psi_i)n_{i+1}}{h_i} - \frac{B(\psi_i - \psi_{i+1})n_i}{h_i} - \frac{B(\psi_i - \psi_{i-1})n_i}{h_{i-1}} + \frac{B(\psi_{i-1} - \psi_i)n_{i-1}}{h_{i-1}} \right] - \left( \frac{h_i + h_{i-1}}{2} \right) R(n, p) = 0 \quad (2.13)$$

and the continuity equation for holes is given by [4]

$$D_p \left[ \frac{B(\psi_i - \psi_{i+1})p_{i+1}}{h_i} - \frac{B(\psi_{i+1} - \psi_i)p_i}{h_i} - \frac{B(\psi_{i-1} - \psi_i)p_i}{h_{i-1}} \right]$$

$$+\frac{B(\psi_i - \psi_{i-1})p_{i-1}}{h_{i-1}}] - (\frac{h_i + h_{i-1}}{2})R(n, p) = 0 \quad (2.14)$$

where B is Bernoulli function and is defined as [4]

$$B(x) = \frac{x}{e^x - 1} \quad (2.15)$$

## 2.4 Discretized equation for the transient condition

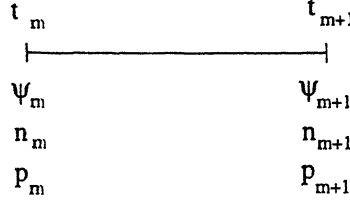
In practical circuits, the external excitation varies with time, hence, electrostatic potential across the diode becomes time dependent and the partial derivatives of the carrier concentration with respect to time does not vanish. The discretization of these equation is obtained using fully backward time differencing (Backward Euler method) scheme. The discretized equations then becomes

$$F_1(\psi_{m+1}, n_{m+1}, p_{m+1}) = 0 \quad (2.16)$$

$$\frac{n_{m+1} - n_m}{d_m} - F_2(\psi_{m+1}, n_{m+1}, p_{m+1}) = 0 \quad (2.17)$$

$$\frac{p_{m+1} - p_m}{d_m} - F_3(\psi_{m+1}, n_{m+1}, p_{m+1}) = 0 \quad (2.18)$$

where  $d_m = t_{m+1} - t_m$ ,  $t_m$  and  $t_{m+1}$  are the two consecutive time steps,  $n_m, p_m$  and  $n_{m+1}, p_{m+1}$  are the concentrations of electrons and holes at time instant  $t_m$  and  $t_{m+1}$  as shown in Fig 2.3,  $F_1$  is Poisson equation,  $F_2$  and  $F_3$  are the continuity equations for electrons and holes respectively. If we substitute the spatial operators in Eq 2.16-2.18, we get completely discretized equations



**CENTRAL LIBRARY**  
**I. I. T., KANPUR**  
**No. A 127973**

Figure 2.3: Change in  $\psi, n$  and  $p$  with time

as

$$\begin{aligned} & \lambda^2 \left[ \psi_{i-1,m+1} \frac{h_{i-1} + h_i}{2h_{i-1}} - \psi_{i,m+1} \left( \frac{h_{i-1} + h_i}{2h_{i-1}} + \frac{h_{i-1} + h_i}{2h_i} \right) \right. \\ & \left. + \psi_{i+1,m+1} \frac{h_{i-1} + h_i}{2h_i} \right] - (n_{i,m+1} - p_{i,m+1} - C_i) = 0 \end{aligned} \quad (2.19)$$

$$\begin{aligned} D_n [ & n_{i-1,m+1} B(\psi_{i-1,m+1} - \psi_{i,m+1}) \frac{h_{i-1} + h_i}{2h_{i-1}} - n_{i,m+1} (B(\psi_{i,m+1} - \\ & \psi_{i-1,m+1}) \frac{h_{i-1} + h_i}{2h_{i-1}} + B(\psi_{i,m+1} - \psi_{i+1,m+1}) \frac{h_{i-1} + h_i}{2h_i} + \frac{1}{d_m}) \\ & + n_{i+1,m+1} B(\psi_{i+1,m+1} - \psi_{i,m+1}) \frac{h_{i-1} + h_i}{2h_i} ] = (R_{i,m+1} - \frac{n_{i,m}}{d_m}) \end{aligned} \quad (2.20)$$

$$\begin{aligned} D_p [ & p_{i-1,m+1} B(\psi_{i,m+1} - \psi_{i-1,m+1}) \frac{h_{i-1} + h_i}{2h_{i-1}} - p_{i,m+1} (B(\psi_{i-1,m+1} - \\ & \psi_{i,m+1}) \frac{h_{i-1} + h_i}{2h_{i-1}} + B(\psi_{i+1,m+1} - \psi_{i,m+1}) \frac{h_{i-1} + h_i}{2h_i} + \frac{1}{d_m}) \\ & + p_{i+1,m+1} B(\psi_{i,m+1} - \psi_{i+1,m+1}) \frac{h_{i-1} + h_i}{2h_i} ] = (R_{i,m+1} - \frac{p_{i,m}}{d_m}) \end{aligned} \quad (2.21)$$

## 2.5 Boundary conditions

The above discretized equations cannot give the values of the electrostatic potential and carrier concentration at the boundary of the device. Hence, the

$$n_R = \frac{n_i^2}{p_L} \quad (2.27)$$

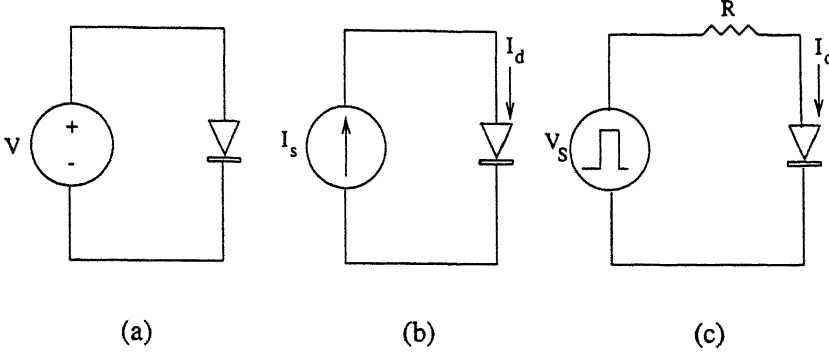


Figure 2.5: Different types of excitations.

For a purely voltage controlled source, Fig 2.5a, if we apply  $V_n$  and  $V_p$  on the left and right hand side boundary respectively, i.e,  $V_{applied} = V_p - V_n$ , the electrostatic potential at the left hand boundary ( $\psi_L$ ) will change to

$$\psi_L = V_n + \psi_L^0 \quad (2.28)$$

and on right hand side boundary electrostatic potential ( $\psi_R$ ) will become

$$\psi_R = V_p - \psi_R^0, \quad (2.29)$$

where  $\psi_L^0$  and  $\psi_R^0$  are the values of the electrostatic potential at equilibrium, and are given by

$$\psi_L^0 = V_T \ln\left(\frac{n_L}{n_i}\right), \quad (2.30)$$

and

$$\psi_R^0 = V_T \ln\left(\frac{p_R}{n_i}\right) \quad (2.31)$$

For a purely current controlled contact, as shown in Fig 2.5b, the value of the electrostatic potential at the right hand boundary can be calculated using

$$\int (J_n + J_p) \cdot dA - I_s(t) = 0 \quad (2.32)$$

$$n_R = \frac{n_i^2}{p_L} \quad (2.27)$$

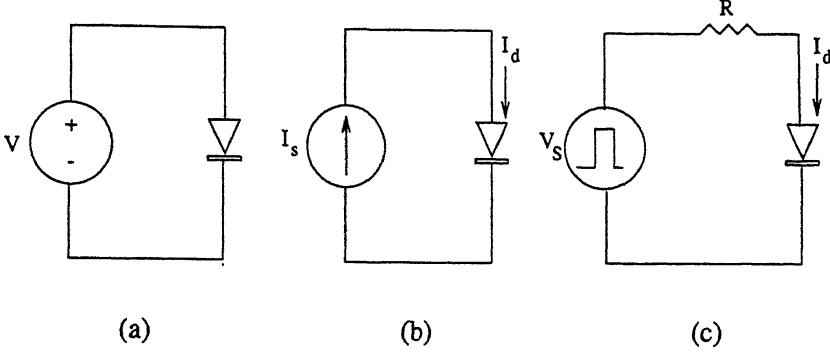


Figure 2.5: Different types of excitations.

For a purely voltage controlled source, Fig 2.5a, if we apply  $V_n$  and  $V_p$  on the left and right hand side boundary respectively, i.e,  $V_{applied} = V_P - V_n$ , the electrostatic potential at the left hand boundary ( $\psi_L$ ) will change to

$$\psi_L = V_n + \psi_L^0 \quad (2.28)$$

and on right hand side boundary electrostatic potential ( $\psi_R$ ) will become

$$\psi_R = V_p - \psi_R^0, \quad (2.29)$$

where  $\psi_L^0$  and  $\psi_R^0$  are the values of the electrostatic potential at equilibrium, and are given by

$$\psi_L^0 = V_T \ln\left(\frac{n_L}{n_i}\right), \quad (2.30)$$

and

$$\psi_R^0 = V_T \ln\left(\frac{p_R}{n_i}\right) \quad (2.31)$$

For a purely current controlled contact, as shown in Fig 2.5b, the value of the electrostatic potential at the right hand boundary can be calculated using

$$\int (J_n + J_p) \cdot dA - I_s(t) = 0 \quad (2.32)$$

where  $A$ =cross sectional area of the device,  $I_s$  is the current which is forced to flow through the device,  $J_n$  and  $J_p$  are the electron and hole current densities respectively, and are given by [4]

$$J_n = D_n \frac{B(\psi_{R-1} - \psi_R)n_{R-1} - B(\psi_R - \psi_{R-1})n_R}{h_{R-1}} \quad (2.33)$$

and

$$J_p = D_p \frac{B(\psi_{R-1} - \psi_R)p_R - B(\psi_R - \psi_{R-1})p_{R-1}}{h_{R-1}} \quad (2.34)$$

After putting the values of  $J_n$  and  $J_p$  in Eq 2.32, the electrostatic potential at the right hand boundary can be calculated. The potential at the left hand boundary ( $\psi_L$ ) is kept same the as the equilibrium value, which is given by

$$\psi_L = V_T \ln(p_L/n_i). \quad (2.35)$$

When the diode is used in a circuit having a load resistance as shown in Fig 2.5c, the boundary conditions for the electrostatic potential are obtained using KVL around the loop, given by

$$V_s - I R - V_D = 0 \quad (2.36)$$

where  $V_D$  is the voltage across the diode, and is given by

$$V_D = \psi_R - \psi_L + V_{bi}, \quad (2.37)$$

where  $V_{bi}$  is the barrier potential and is given by

$$V_{bi} = \psi_L^0 + \psi_R^0. \quad (2.38)$$

After the boundary conditions are established, the nonlinear equations are solved by the Newton-Raphson method [6].

where  $A$ =cross sectional area of the device,  $I_s$  is the current which is forced to flow through the device,  $J_n$  and  $J_p$  are the electron and hole current densities respectively, and are given by [4]

$$J_n = D_n \frac{B(\psi_{R-1} - \psi_R)n_{R-1} - B(\psi_R - \psi_{R-1})n_R}{h_{R-1}} \quad (2.33)$$

and

$$J_p = D_p \frac{B(\psi_{R-1} - \psi_R)p_R - B(\psi_R - \psi_{R-1})p_{R-1}}{h_{R-1}} \quad (2.34)$$

After putting the values of  $J_n$  and  $J_p$  in Eq 2.32, the electrostatic potential at the right hand boundary can be calculated. The potential at the left hand boundary ( $\psi_L$ ) is kept same the as the equilibrium value, which is given by

$$\psi_L = V_T \ln(p_L/n_i). \quad (2.35)$$

When the diode is used in a circuit having a load resistance as shown in Fig 2.5c, the boundary conditions for the electrostatic potential are obtained using KVL around the loop, given by

$$V_s - I R - V_D = 0 \quad (2.36)$$

where  $V_D$  is the voltage across the diode, and is given by

$$V_D = \psi_R - \psi_L + V_{bi}, \quad (2.37)$$

where  $V_{bi}$  is the barrier potential and is given by

$$V_{bi} = \psi_L^0 + \psi_R^0. \quad (2.38)$$

After the boundary conditions are established, the nonlinear equations are solved by the Newton-Raphson method [6].

# Chapter 3

## Results and discussion

The simulation method as described in Chapter 2 can give the results for any arbitrary doping profile and external excitation. In the present work we have chosen abrupt doping profile because most of the analytical solutions are available for this type of profile. A sample device structure is shown in Fig 3.1.

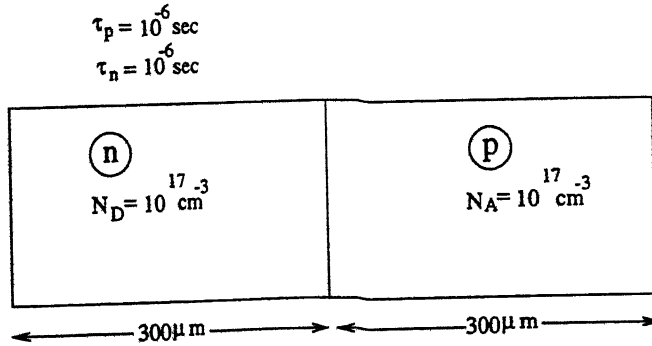


Figure 3.1: Sample

The length of the  $p$  side and  $n$  side of the diode are chosen  $\sim 5L_n$  and  $\sim 5L_p$

respectively so that the minority carriers should recombine before reaching the diode boundary.

### 3.1 Turn on transient

The phenomena occurring inside the device for the small current step and the high current step are quite different, which are explained in the following sections. The turn ON excitation (current or voltage) is shown in the Fig 3.2. It is defined as

$$u(t) = \begin{cases} 0 & \text{if } t < 0 \\ F & \text{if } t > 0 \end{cases}$$

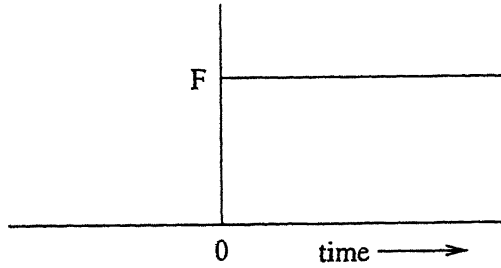


Figure 3.2: Turn ON step.

#### 3.1.1 Small current step

A small current step is recognized as the excitation causing low level injection on either side of the junction. We have chosen

$$J(t) = \begin{cases} 0 & \text{if } t < 0 \\ 10 \text{ Amp cm}^{-2} & \text{if } t > 0 \end{cases}$$

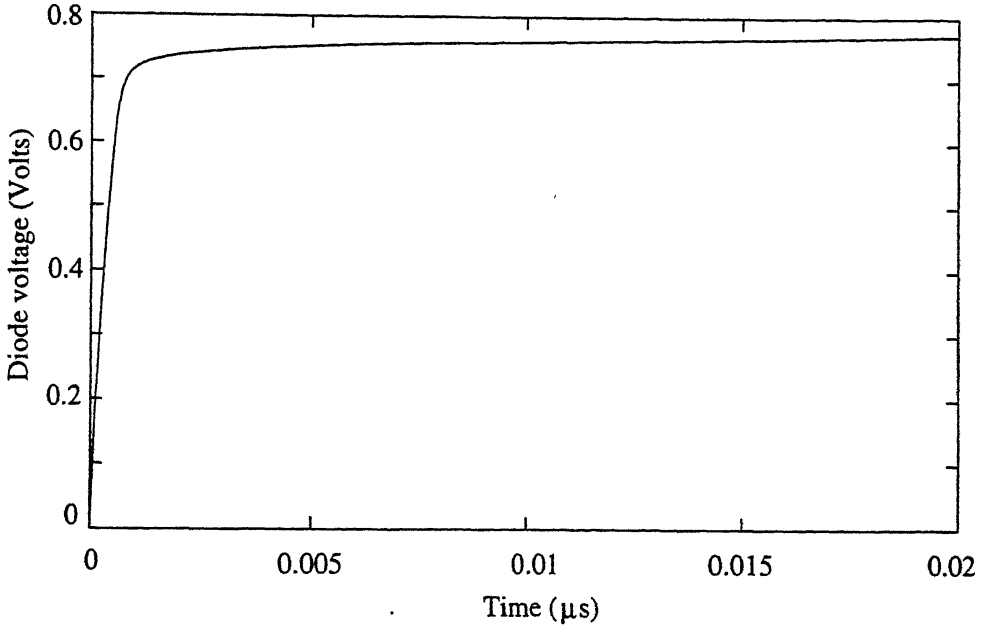


Figure 3.3: Variation of diode voltage with time for small current step.

For the above given current the injection level is of the order of  $10^{14} \text{ cm}^{-3}$  (Fig 3.7, in all the subsequent figures  $t_1 = 1 \text{ ns}$ , where  $t_1$  is the time after the rising edge and each subsequent curve is  $\Delta t \text{ ns}$  apart, where  $\Delta t = 1 \text{ ns}$ ), hence it is verified that the injection level is low. The voltage response for this excitation is shown in the Fig 3.3. The voltage waveform does not show an abrupt rise due to the charging of the transition capacitance [7]. The diffusion capacitance has insignificant influence on the transient response at low level injection. In the initial part, the transition region capacitance is charged by the displacement current because initially the displacement current is vary high in the transition region. In Fig 3.4 the displacement current is shown as a function of position and time. It has significant values near the junction because the variation in the electric field with time is significant only in this region. At later times, electron and hole currents become dominant components and the displacement current charging the transition region capacitance gradually decreases to zero. The variation of the electron and hole current in

the neutral  $p$  region are shown in Figs, 3.5 and Fig 3.6 respectively.

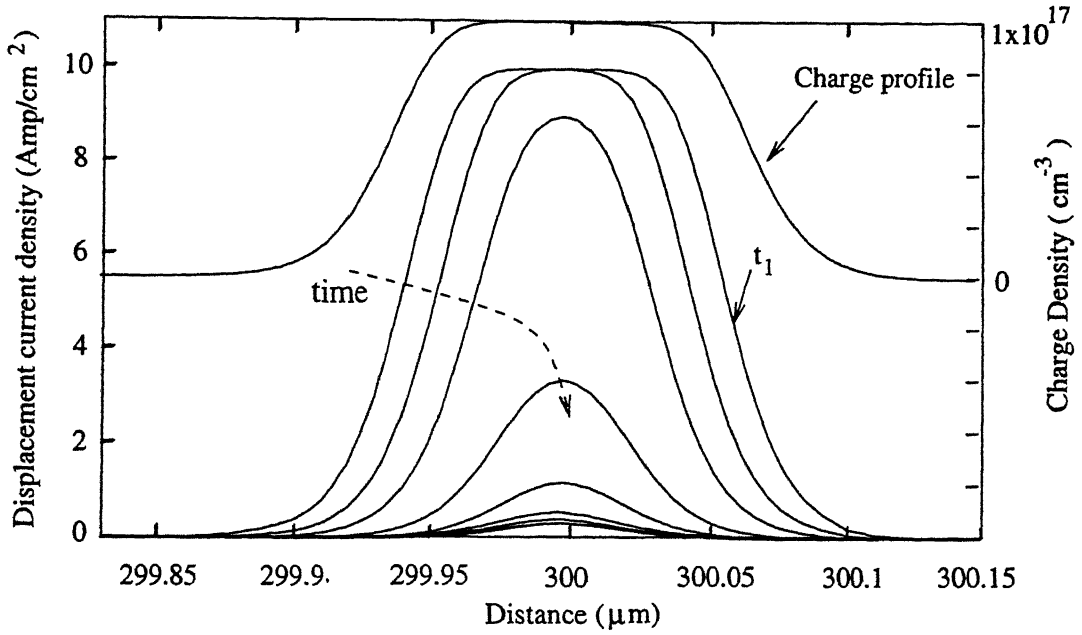


Figure 3.4: Displacement current density vs distance for small current step.

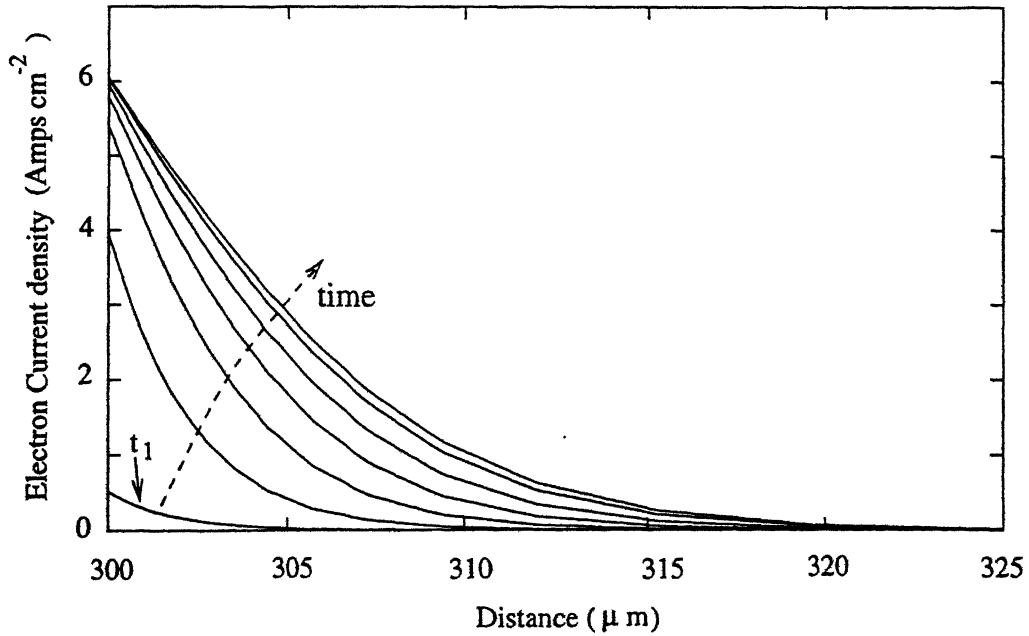


Figure 3.5: Electron current density vs distance for small current step.

From Figs 3.4-3.6, it can be seen that initially the transition region is

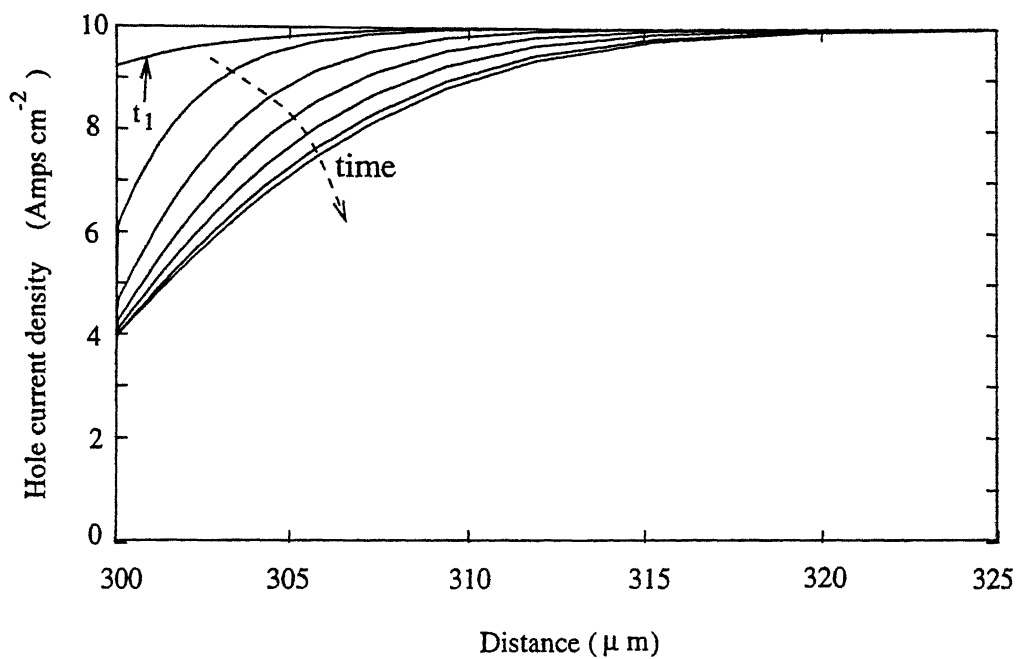


Figure 3.6: Hole current density vs distance for small current step.

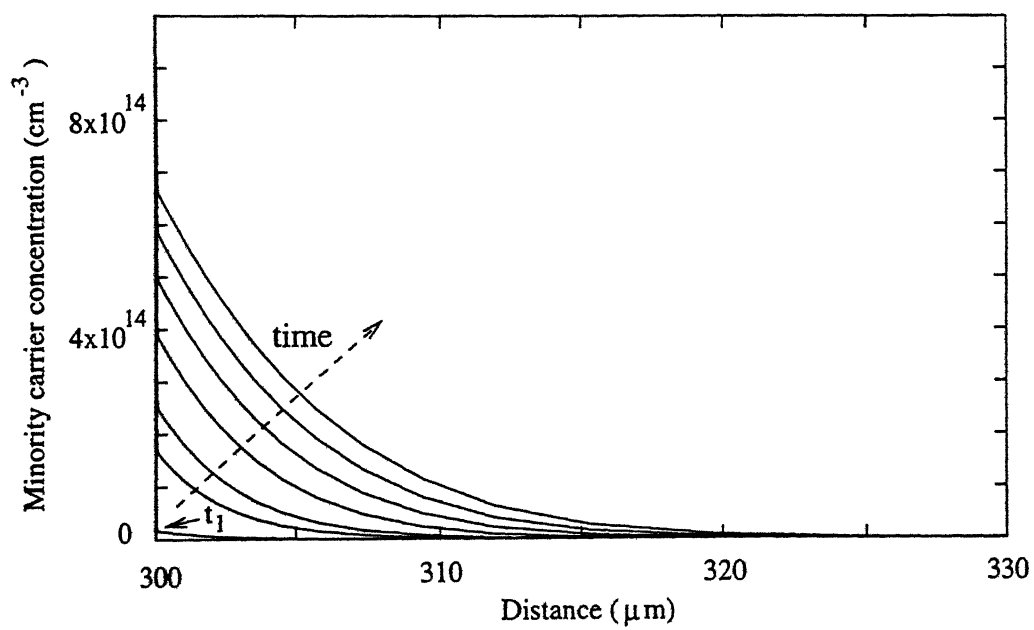


Figure 3.7: Minority carrier (electrons on *p* side) concentration vs distance for small current step.

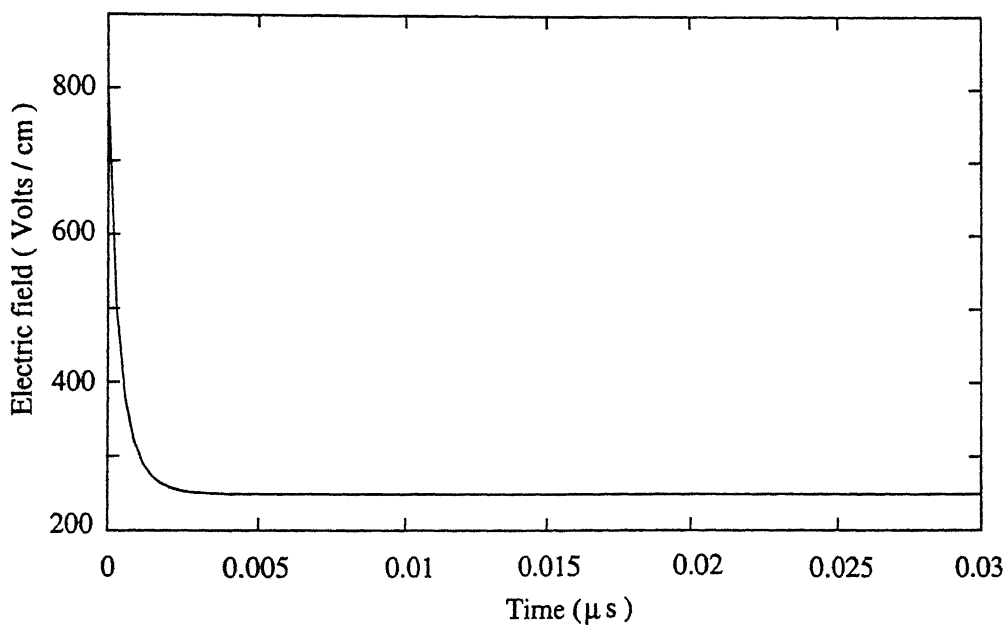


Figure 3.8: Electric field (at  $x= 300.0022 \mu m$ ) vs time for small current step.

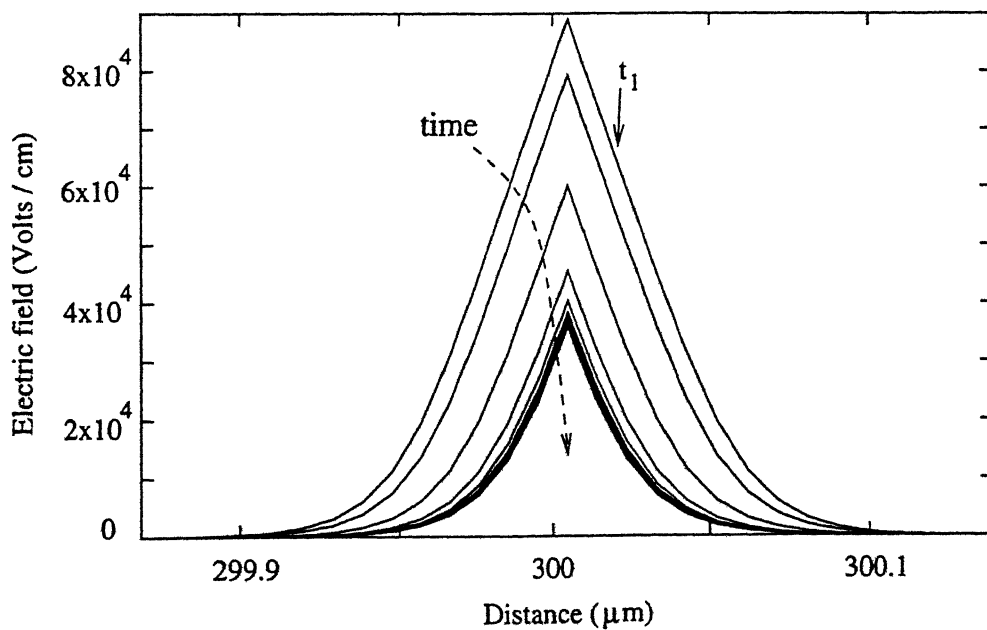


Figure 3.9: Electric Field vs distance for small current step.

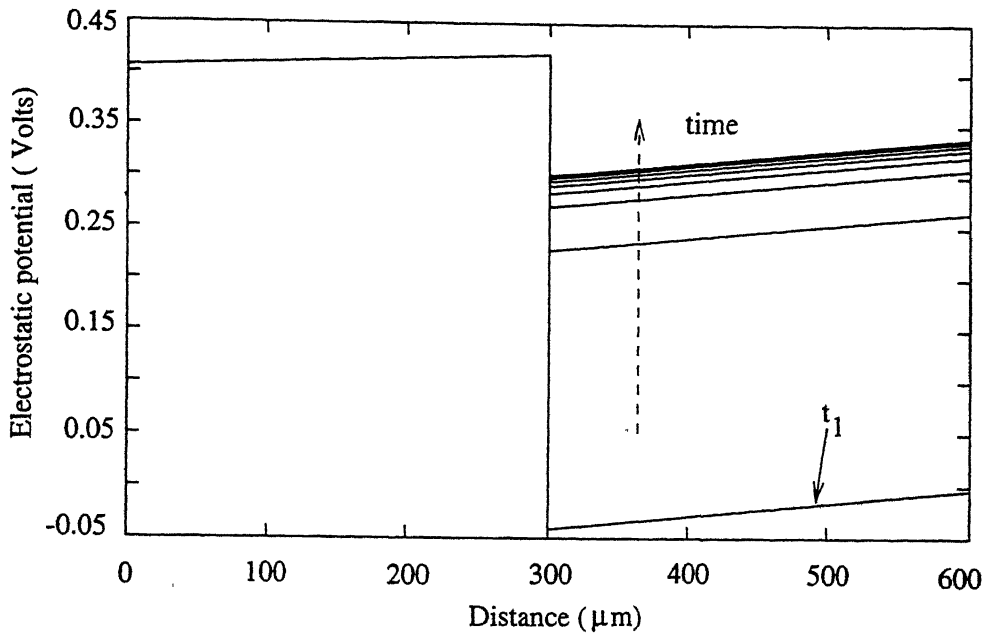


Figure 3.10: Electrostatic potential vs distance for small current step.

dominated by the flow of displacement current. The electron and hole current components are very less in this region due to the little change of electric field and the mobile carrier densities from the initial equilibrium value (minority carriers on the  $p$  side are shown in Fig 3.7) while the variation of the electric field with time is large as shown in Fig 3.8. The variation of electric field with distance at different times is shown in the Fig 3.9. The decrease in the electric field in the transition region is related to the change of junction voltage. The electric field is maximum at the junction due to the maximum variation of electrostatic potential at that point. The electrostatic potential with respect to distance curve is shown in Fig 3.10. We see that due to some finite resistance of the neutral region the electrostatic potential curve is not constant in the neutral region.

### 3.1.2 High current step

We have taken the following as a high current step

$$J(t) = \begin{cases} 0 & \text{if } t < 0 \\ 500 \text{ Amp cm}^{-2} & t > 0 \end{cases}$$

When it is applied to the device, initially in thermal equilibrium, the final state is high injection level. The minority carrier concentration is  $\sim 0.6.N_A$  (as shown in the Fig 3.16), which confirms high level injection. The variation of the diode voltage with time is shown in Fig 3.11. The initial part is the result of combination of two basic effects : the buildup of the ohmic voltage drop in the neutral regions and the charging of the transition region capacitance. In the high level injection the motion of the carriers is ruled by both drift and diffusion phenomena, as a result of conductivity modulation. The displacement currents at various instants of time in the transition region and the neutral region respectively are shown in Figs. 3.12 and 3.13.

We see that this is different from the small current excitation. Figure 3.12 shows the displacement current in the transition region. Due to the very small width of the transition region, the displacement current is nowhere constant as opposed to Fig 3.4 (where it is constant in the depletion region) for small current step, where the depletion width is larger than the present case. Figure 3.13 shows the variation of displacement current in the neutral region at different time instants. The reversal of the direction of the displacement current flow is a consequence of decrease of voltage drop in the quasi neutral region because conductivity modulation is occurring in this region. The modulation initiates at the edge of the transition region and evolves gradually towards the

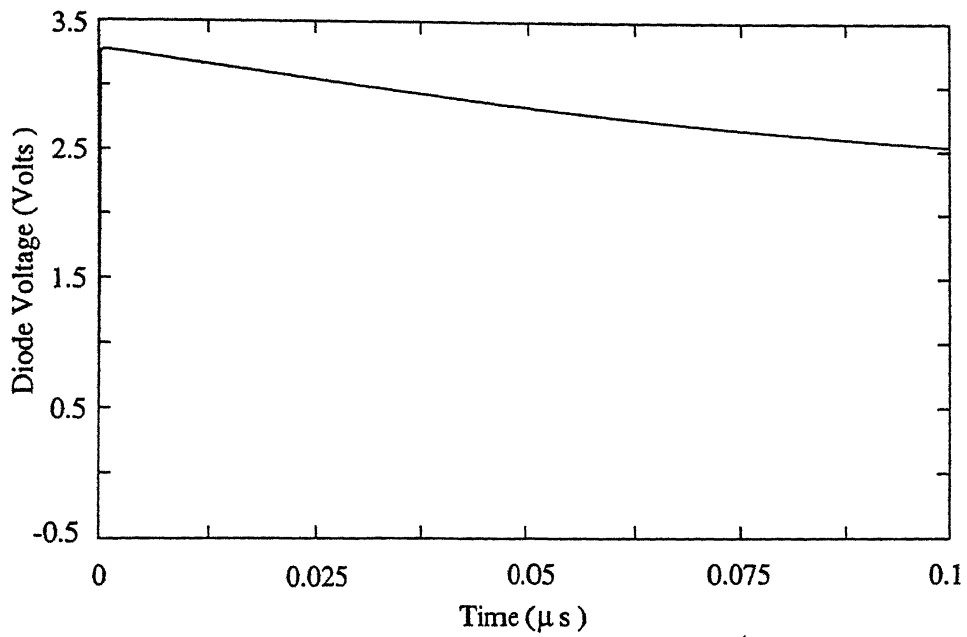


Figure 3.11: Diode voltage vs time for high current step.

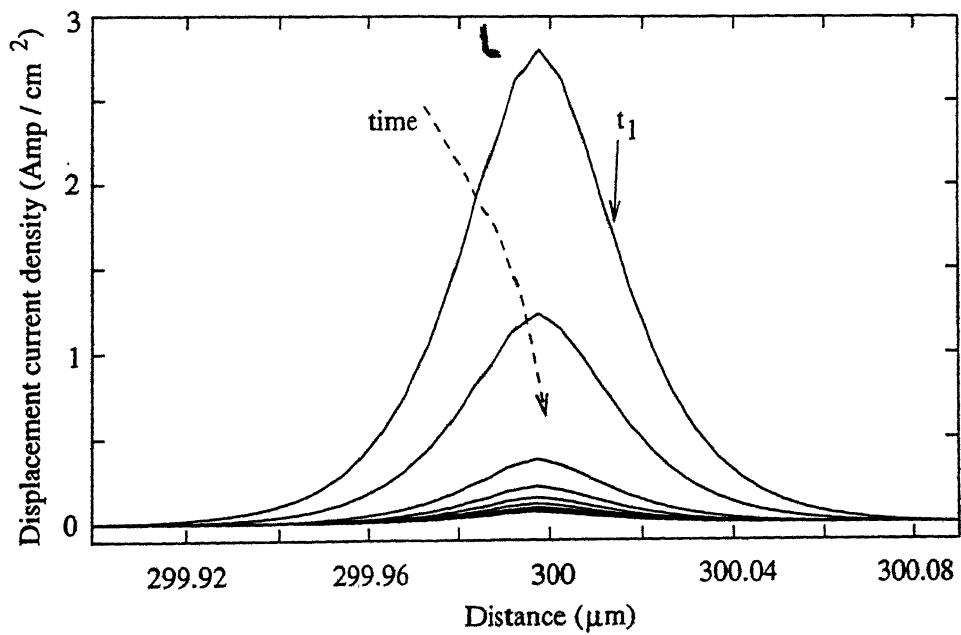


Figure 3.12: Displacement current density vs distance for high current step in the transition region.

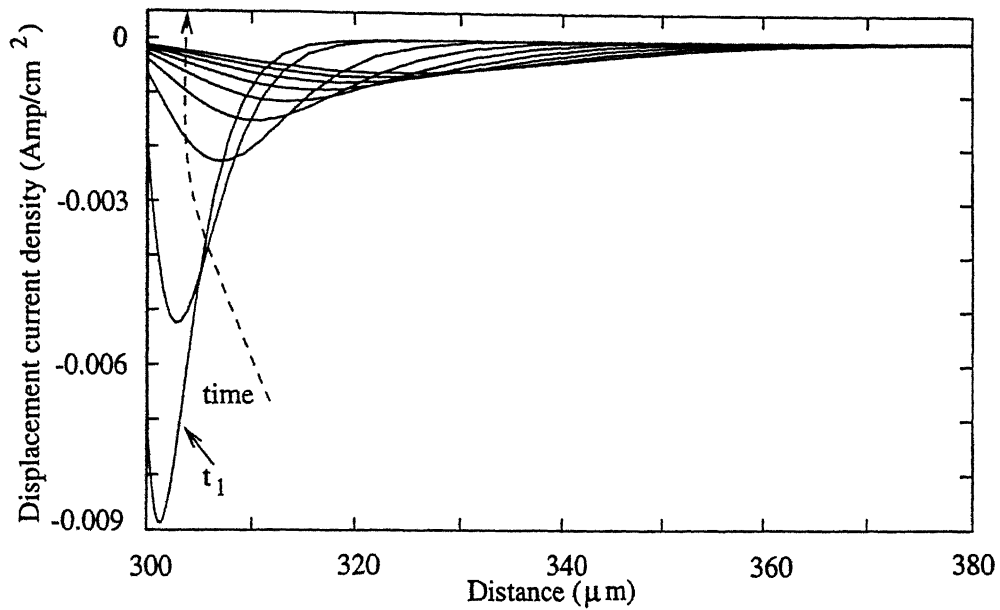


Figure 3.13: Displacement current density vs distance for high current step in the neutral region

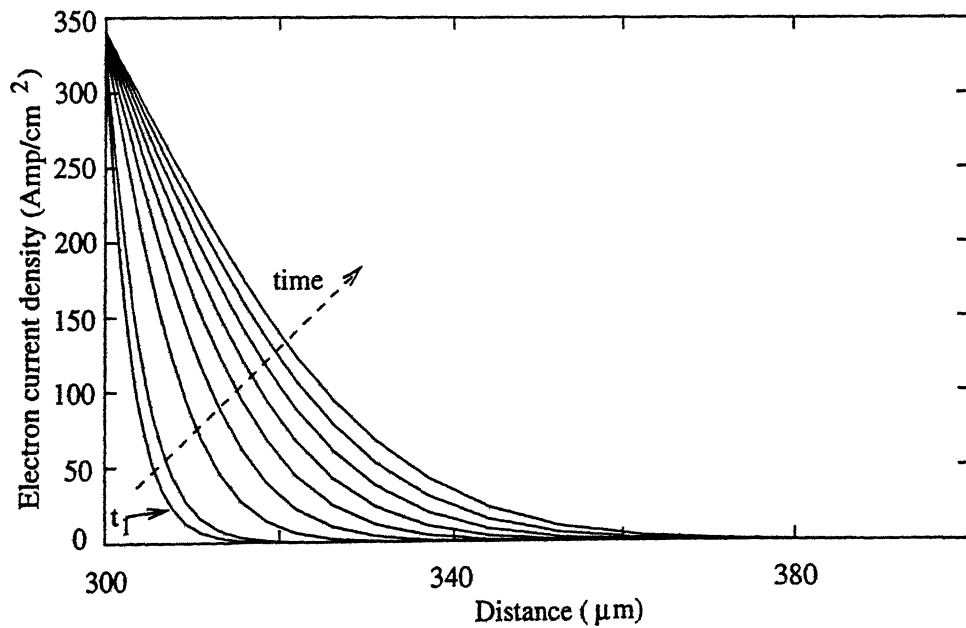


Figure 3.14: Electron current density vs distance for high current step.

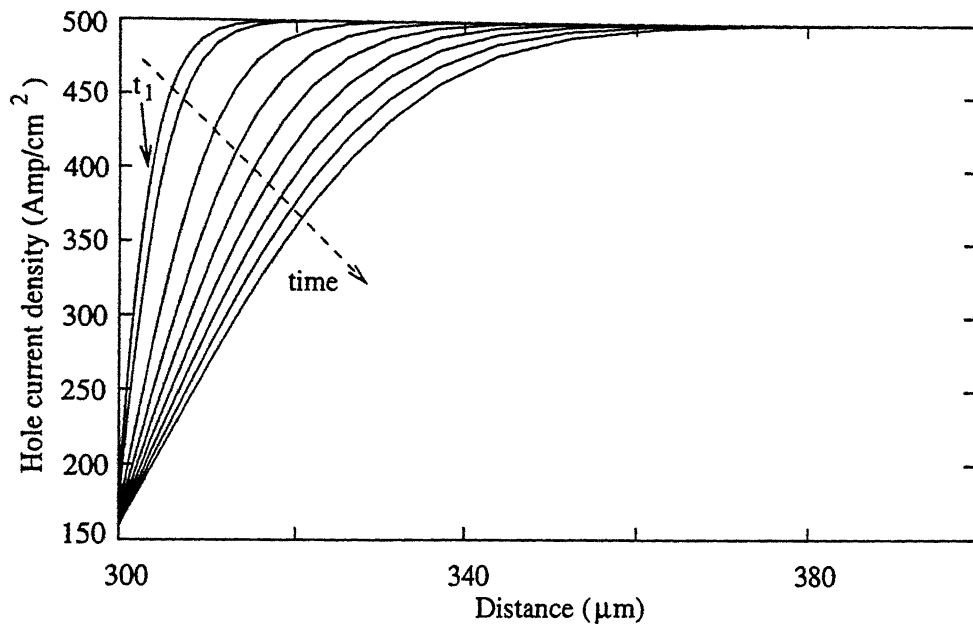


Figure 3.15: Hole current density vs distance for high current step.

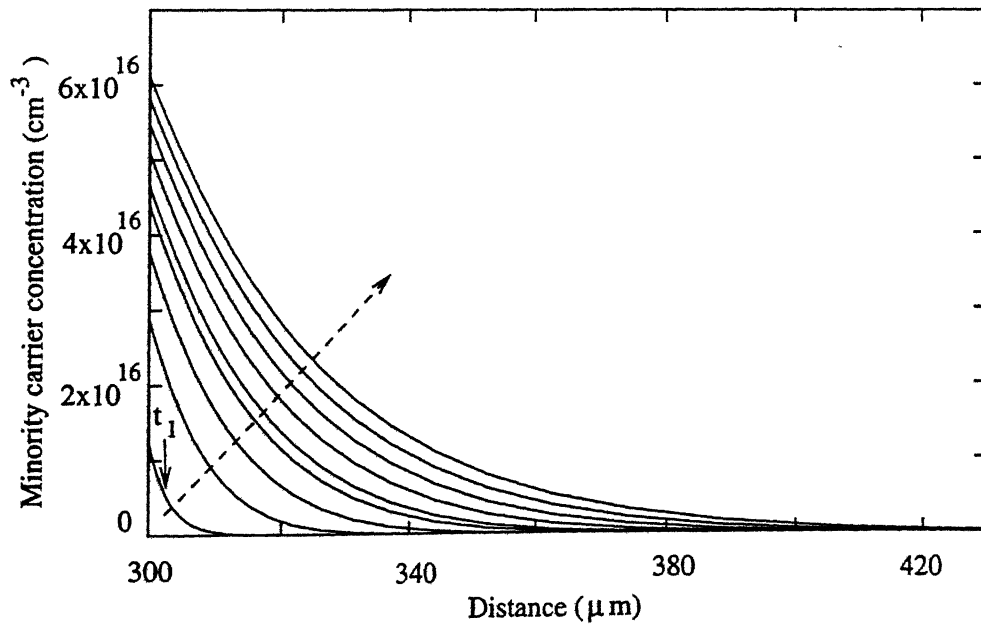


Figure 3.16: Minority carrier (electrons on *p* side) concentration vs distance for high current step.

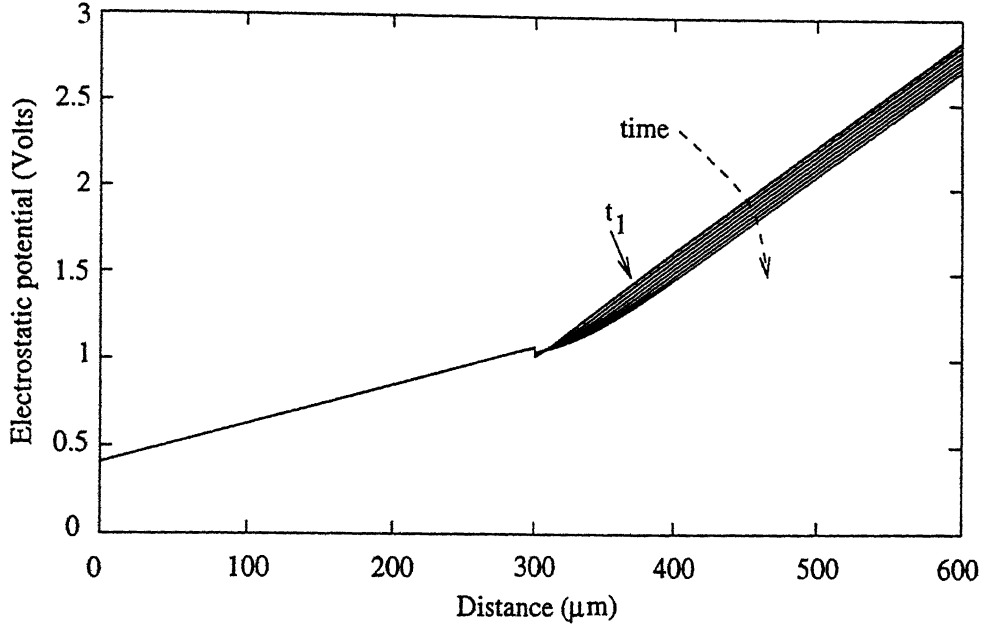


Figure 3.17: Electrostatic potential vs distance for high current step.

external contacts [7].

Figures 3.14 and 3.15 show the electron and hole current distributions on  $p$  side. We see that the slopes near the edge of the transition region is higher than those for small current step (Figs 3.5 and 3.6).

The variation of the electrostatic potential is shown in Fig. 3.17. Due to the large voltage drop in the neutral region the slope of the electrostatic potential is high.

### 3.1.3 Voltage step

A voltage step (0 to 0.3 Volts) is applied to the diode without any load resistance to see the variation of the minority carrier concentration. For a voltage step, the variation of the diode current is shown in Fig 3.18. We

see that initially the current rises very sharply, this is due to the transition region capacitance (it acts as short circuit). Hence, initially the displacement current is also significant (Fig 3.19). As time progresses, the transition region capacitance starts to charge and the displacement current decreases, the total current also reaches the steady state value. The electrostatic potential is shown in Fig 3.20. Its variation occurs in the neutral region near the junction. The excess minority carrier concentration is shown in Fig 3.21. The excess electron concentration near the junction changes from zero to  $n_{p0}[\exp(V_F/V_T) - 1]$ . Since the electrons cannot diffuse into neutral  $p$  region just after the turn ON step, the slope of the excess electron concentration at the edge of the transition region at the  $p$  side  $((\delta n/\delta x)|_{x=x_p})$  will be large just after the turn ON step, hence this is also a reason for the initial high current through the diode, and slowly as the minority carrier concentration increases the slope decreases and thus the current decreases [8].

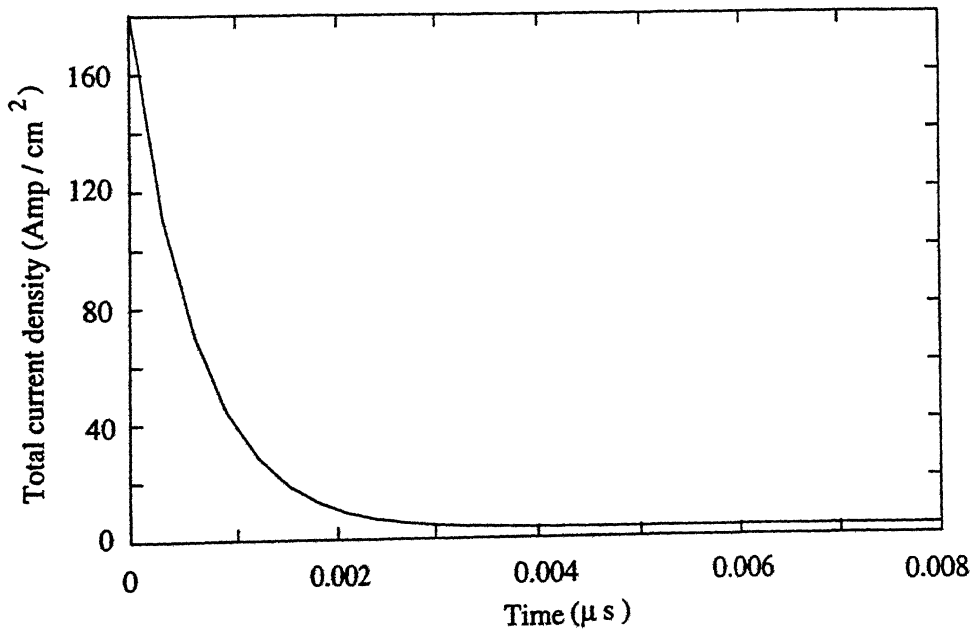


Figure 3.18: Variation of diode current vs time for voltage step.

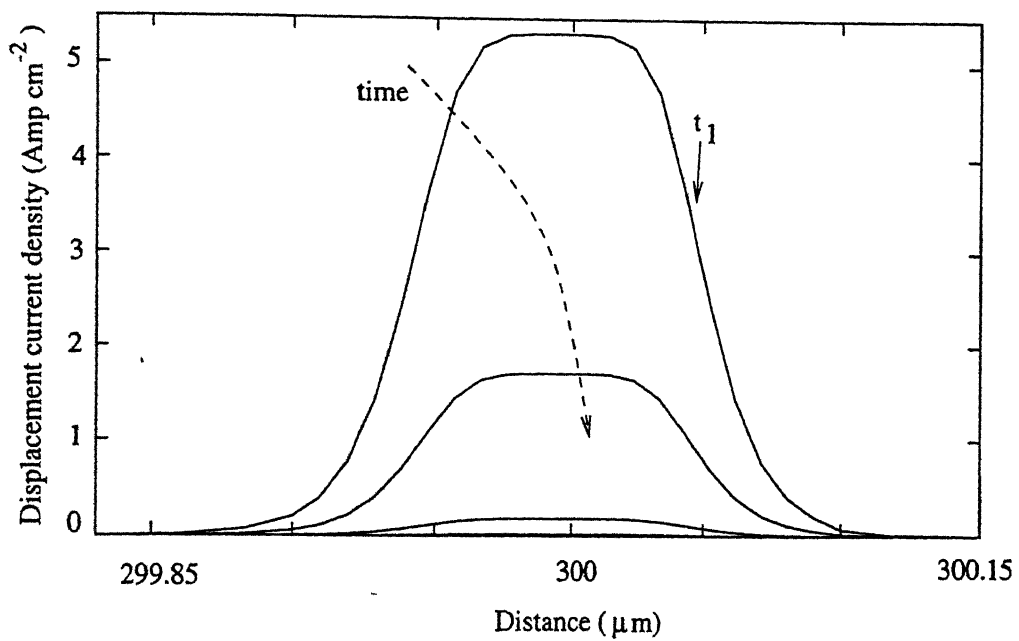


Figure 3.19: Displacement current density vs distance for voltage step.

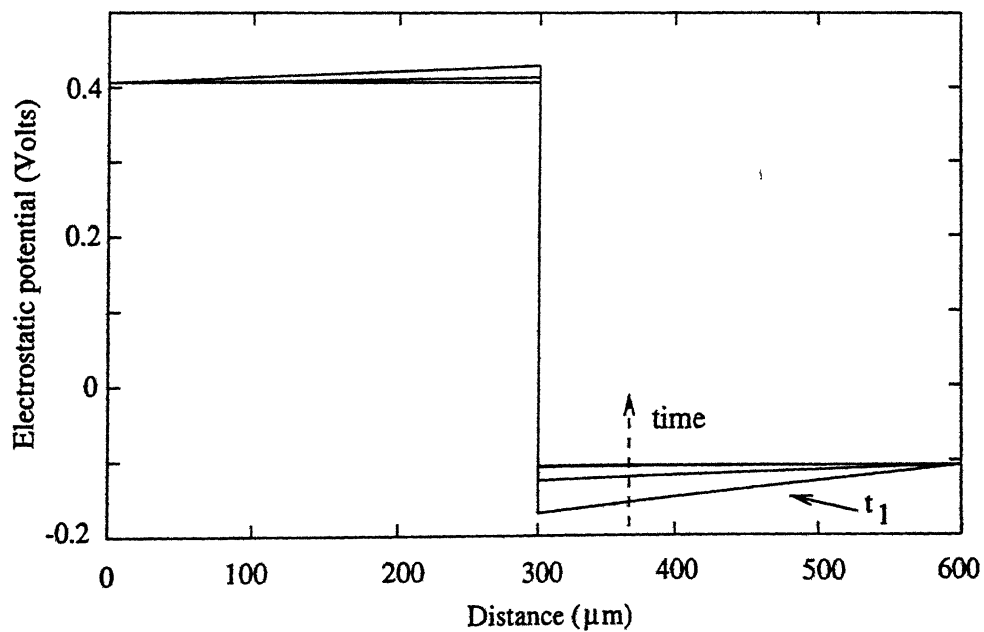


Figure 3.20: Electrostatic potential vs distance for voltage step.

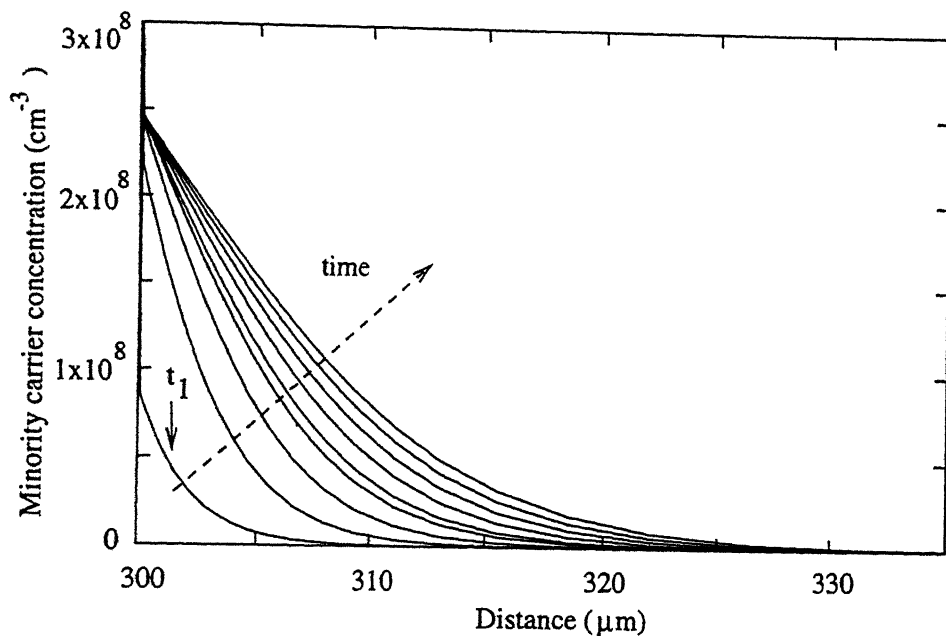


Figure 3.21: Minority carrier concentration (electrons on  $p$  side) vs distance for voltage step.

## 3.2 Turn off transient

The turn OFF step is shown in Fig 3.22a. For the turn off transient we have taken the circuit shown in the Fig 2.5c (Chapter 2), for analyzing the storage and fall time delay of the current through the diode, by varying different circuit parameters. The diode chosen is  $n^+p$  for comparison with the analytical expressions.

The applied input voltage and the diode responses are shown in the Fig 3.22. Initially when the applied voltage is 10 Volts, the diode is forward biased and steady state current of 4.5 Amps is flowing (Fig 3.22c) through it. At time  $t_1$ , the diode voltage is reversed to -5 Volts. The diode voltage reduces (Fig 3.22b), but does not reverse. The current does not drop to zero, it reverses and remains at  $\sim V/R_L$  because the minority carriers cannot recover immediately.

At time  $t_2$  when the excess minority carriers in the immediate neighborhood of the junction have been swept back across the junction, the diode voltage starts to reverse and the magnitude of the diode current begins to decrease. From Fig 3.22d we see that from time  $t_1$  to  $t_2$  the rise in electric field is small because the transition width does not changes significantly, it starts rising only after time  $t_2$ .

The analytical formulae used for calculating storage delay time [9] and fall time [10] are as follows:

$$\tau_s = \tau_n [\operatorname{erfc}(\frac{1}{1 + I_R/I_F})]^2 \quad (3.1)$$

$$\operatorname{erf}\sqrt{\frac{\tau_F}{\tau_n}} + \frac{\exp(\frac{-\tau_F}{\tau_n})}{\sqrt{\frac{\pi\tau_F}{\tau_n}}} = 1 + 0.1(\frac{I_R}{I_F}) \quad (3.2)$$

where  $\tau_n$  is electron lifetime,  $\tau_s$  is storage delay time,  $\tau_F$  is fall time,  $I_R$ = reverse current and  $I_F$ = forward current. The effect of the variation of the load resistance on current is shown in Fig 3.23. We see that the storage time and the fall time delay remain constant. This is because the ratio of the forward current (which is injecting the minority carriers) and the reverse current (which is withdrawing the minority carriers) remains constant.

Figure 3.24 shows the variation of the current if the reverse bias is increased, keeping forward bias constant. We see that as the reverse bias is increased, both storage time and fall time decrease, which is due to the increase in the reverse current. As the reverse current increases, the minority carriers are swept back quickly. The variations of the storage time and the fall time delays are shown in the Figs. 3.25 and 3.26 respectively. When keeping reverse bias constant and forward bias changing, the current varies as shown in Fig.3.27. We see that the storage and the fall time delays are increasing. This is because of increased forward current and thereby increase in injected excess minority

carriers. The reverse current is constant, hence, more time is required to withdraw the excess minority carriers when the forward bias are larger. The increase of storage and fall time delays with increase in forward bias are shown in Figs 3.28 and 3.29 respectively. The analytical expression values of storage delay time agrees well with the simulated results but there is large difference between the analytical results for fall time and the simulated results. This difference can be due to the fact that the change of the transition region width is not taken into account properly when deriving the analytical expression.

For studying the variation of the storage delay time and fall time with respect to lifetime ( $\tau_n$  and  $\tau_p$ ), we have taken a long base  $pn$  diode with  $N_A=N_D=10^{17} \text{ cm}^{-3}$ , so that we can see the minority carrier distribution properly (in case of  $n^+p$  diode, holes on the  $n$  side are very small as compared to electrons on the  $p$  side) on the falling edge of the input voltage. Figure 3.30 shows the decay of minority carriers for different values of  $\tau_n$  and  $\tau_p$ . In Fig 3.30a,  $\tau_n = \tau_p$ , we see that on both sides decay of excess minority carriers is occurring at the same rate and reaching zero at the same time. In Fig 3.30b,  $\tau_n = 4 \tau_p$ , hence electrons on  $p$  side are decaying slowly compared to holes on  $n$  side. In Fig 3.30c,  $\tau_p = 4 \tau_n$ , therefore the holes on  $n$  side decay slowly compared to electrons on  $p$  side.

The peak concentration of the minority carriers at the edge of the depletion region boundary is also increased. It can be explained as follows: suppose the forward current is assumed to be constant at  $\sim (V_s/R_L)$ , then  $J_n = \frac{D_n q \delta n(x)}{L_n}$ , and from this equation we can write  $\delta n(x) \propto J_n \sqrt{\tau_n}$ . Therefore, the excess minority carriers will increase as  $\tau_n$  is increased, while the current is constant. A similar explanation for Fig 3.30c, where  $\tau_p = 4 \tau_n$ , can be given. The variation of the storage delay time and fall time with respect to  $\tau_n/\tau_p$  is shown

in Figs 3.31 and 3.32 respectively.

### 3.3 Comparison with SPICE

For comparison with SPICE [11], a short base diode is taken for simulation because SPICE uses short base diode model. The circuit used is shown in Fig 2.25c ( where forward voltage= 10 Volts, reverse voltage= -2 Volts). The parameters required in SPICE, i.e., transit time ( $TT = \frac{W_p^2}{2D_n}$ ) where  $W_p$  is the width of  $p$  side, junction voltage (VJ), reverse saturation current (IS), parasitic resistance (RS), and zero bias  $pn$  capacitance (CJO) are kept the same as those which are used in simulation. The current versus time plot is shown in Fig 3.33.

It is seen that SPICE gives very high value of the storage time delay. It is almost five times the simulated value. On the other hand SPICE gives negligible fall time while simulated results gives finite amount of fall time . This difference is probably due to the fact that, the decay of minority carrier concentration as a function of time is rather complicated as shown if the Fig 3.34. In SPICE, only simple approximation is used to describe the minority carrier concentration. The difference for fall time delay is due to the improper capacitance modelling.

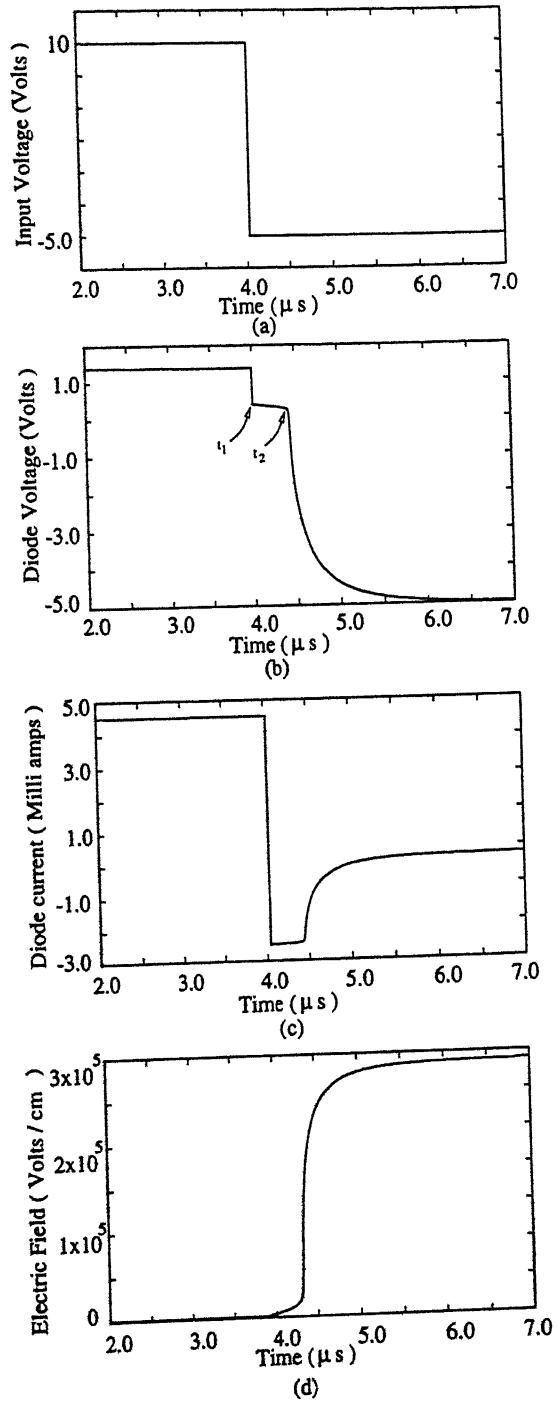


Figure 3.22: (a) Input Voltage vs time; (b) Diode Voltage vs time; (c) Diode Current vs time; (d) Electric field near the junction vs time.

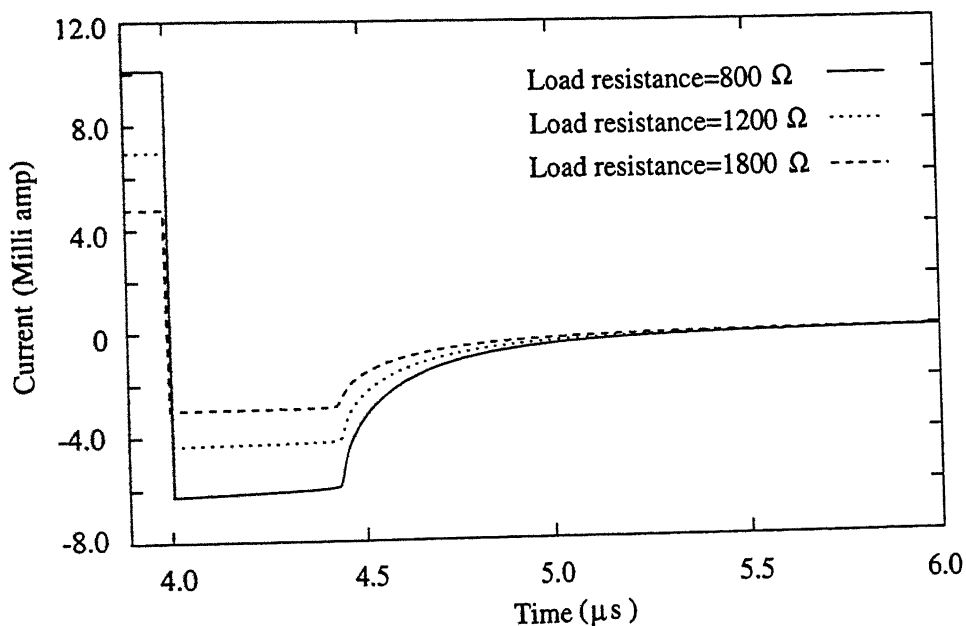


Figure 3.23: Turn off transient of the diode current vs time for different external load, keeping the forward and the reverse bias constant.

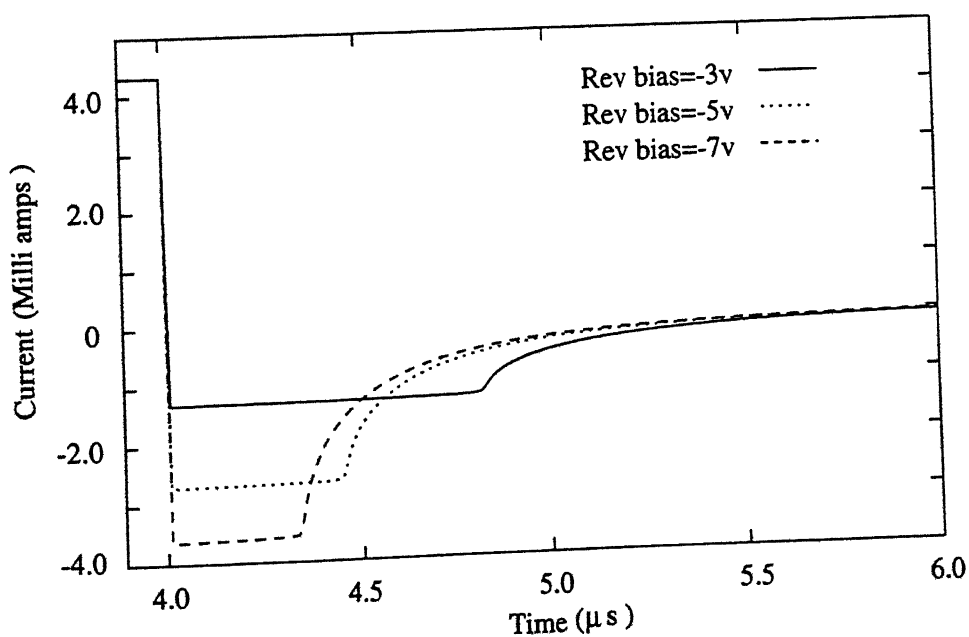


Figure 3.24: Turn off transient of the diode current vs time for different reverse biases, keeping the forward bias constant.

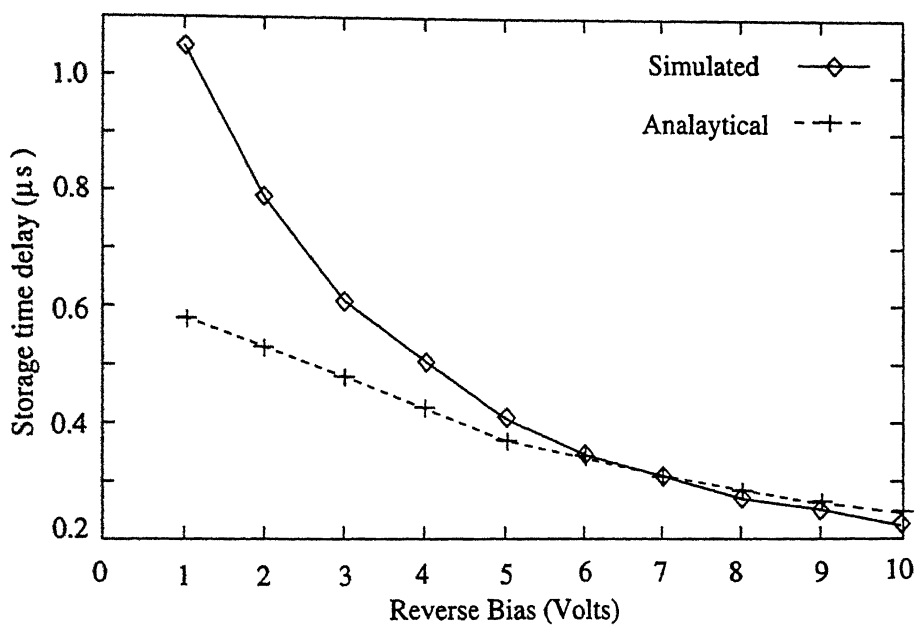


Figure 3.25: Storage time delay vs Reverse bias.

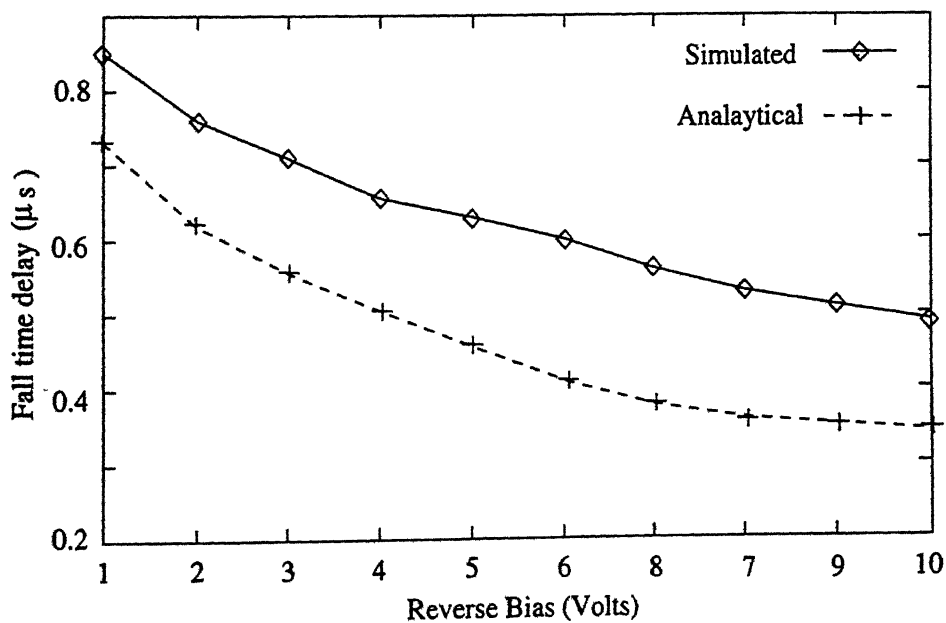


Figure 3.26: Fall time delay vs Reverse bias.

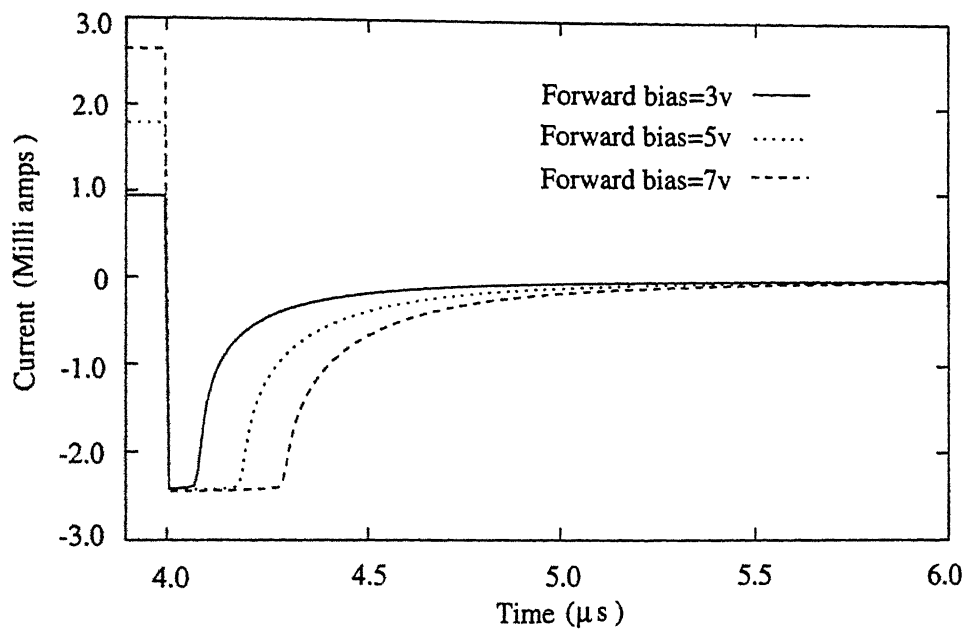


Figure 3.27: Turn off transient of the diode current vs time for different forward biases, keeping the reverse bias constant.

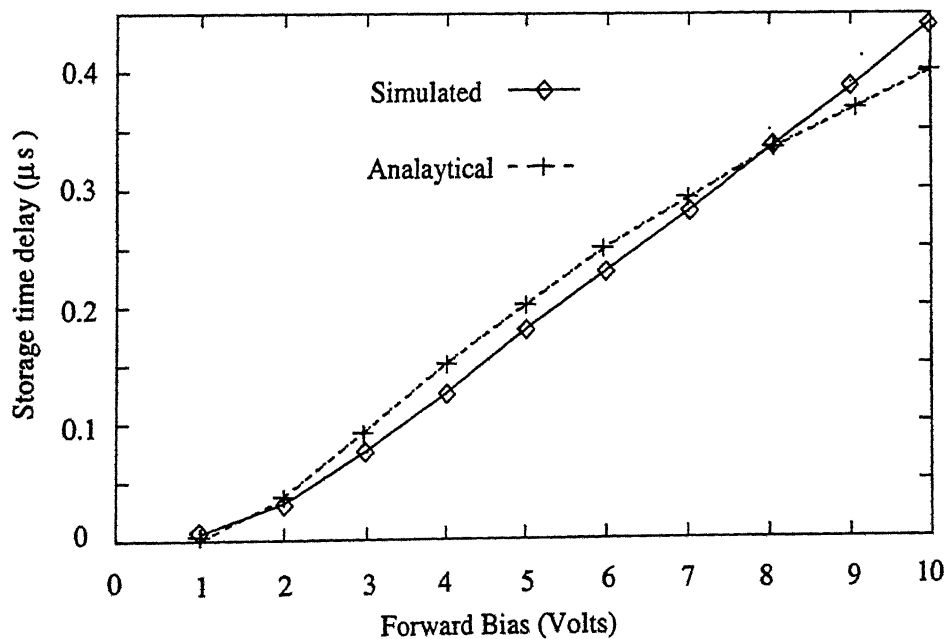


Figure 3.28: Storage delay time vs Forward bias.

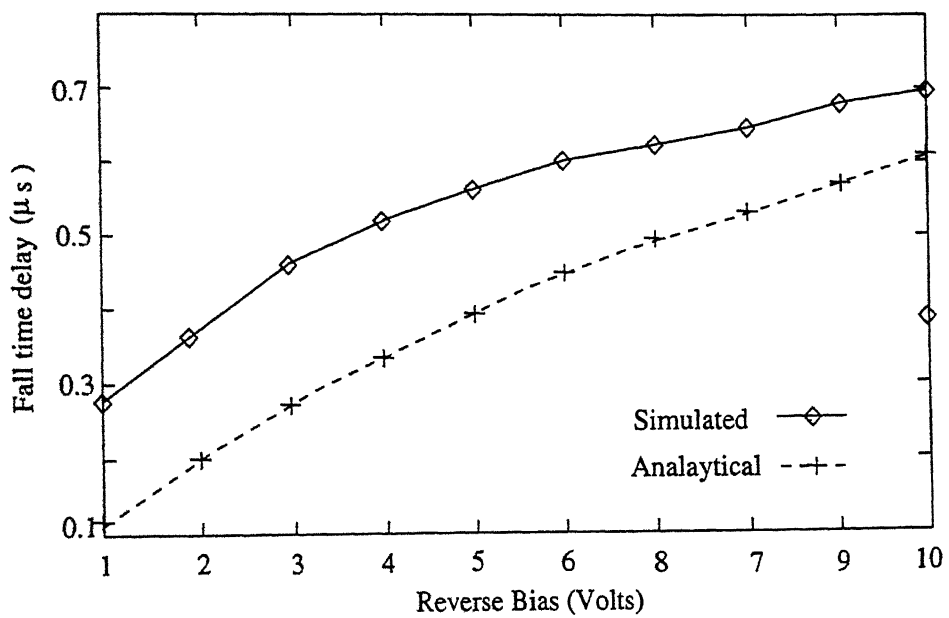


Figure 3.29: Fall time delay vs Forward bias.

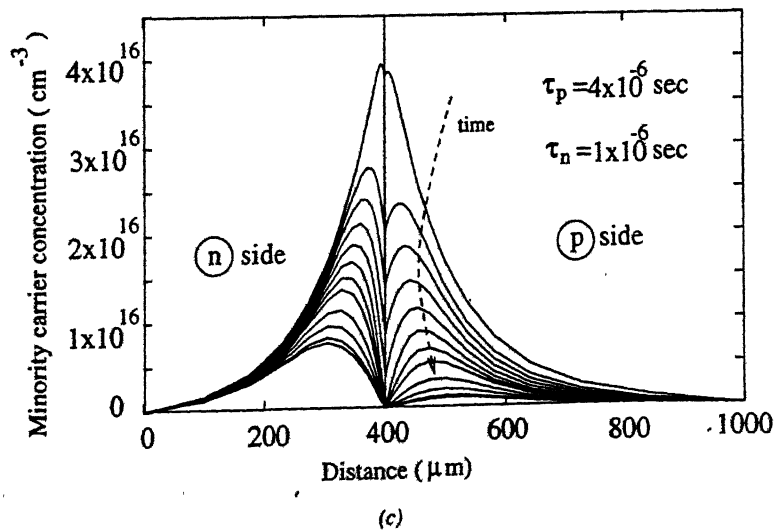
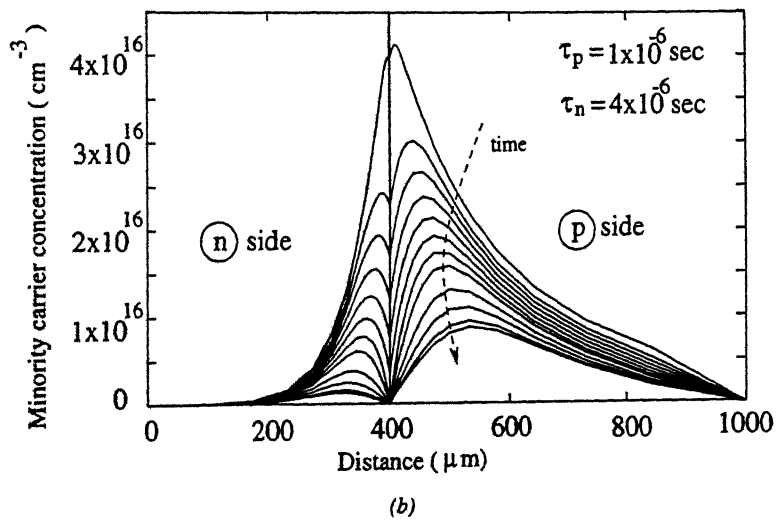
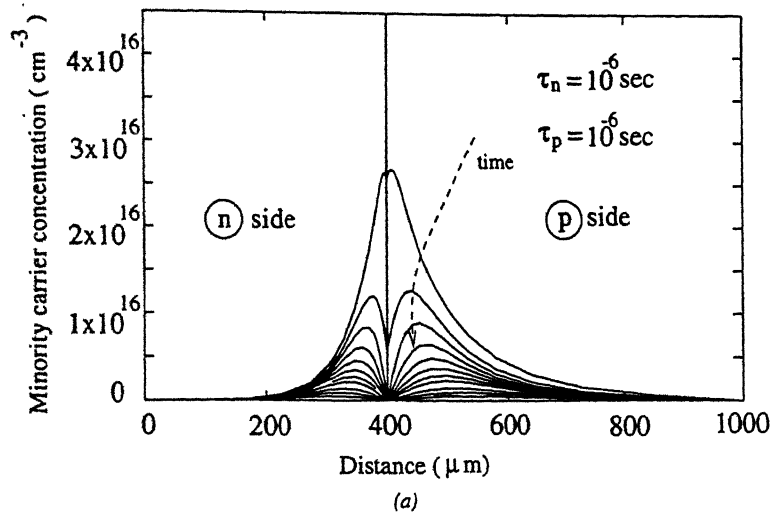


Figure 3.30: Minority carriers concentration vs distance for different values of  $\tau_n$  and  $\tau_p$

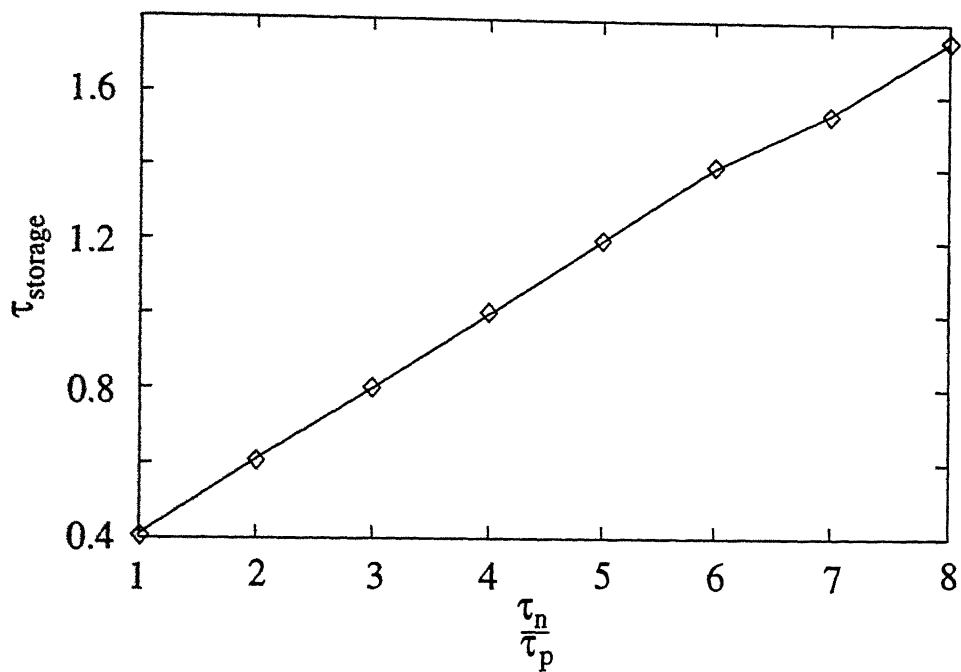


Figure 3.31: Storage time delay vs  $\tau_n/\tau_p$ .

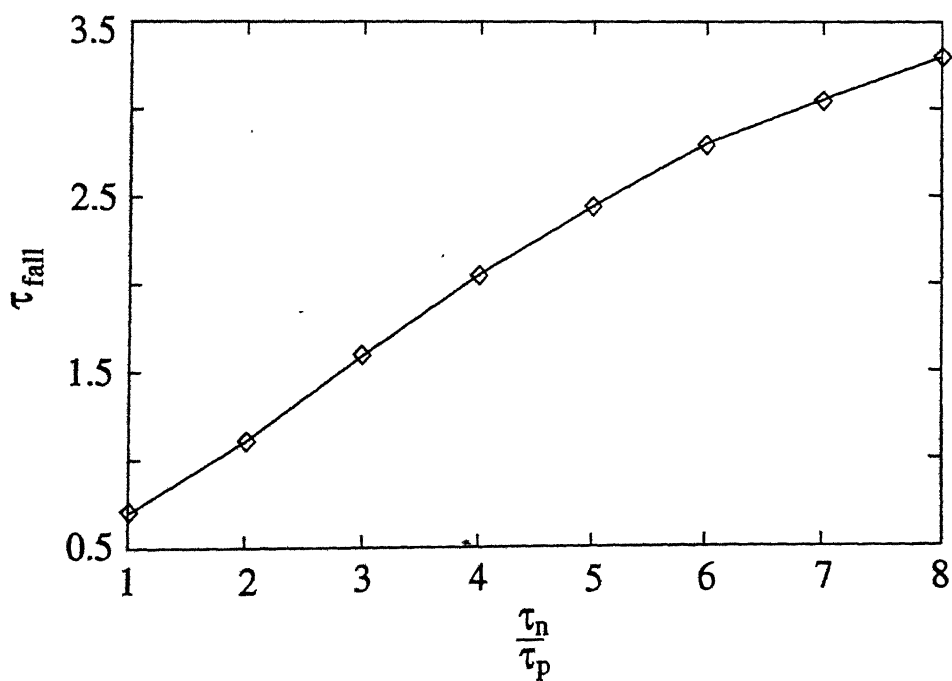


Figure 3.32: Fall time delay vs  $\tau_n/\tau_p$ .

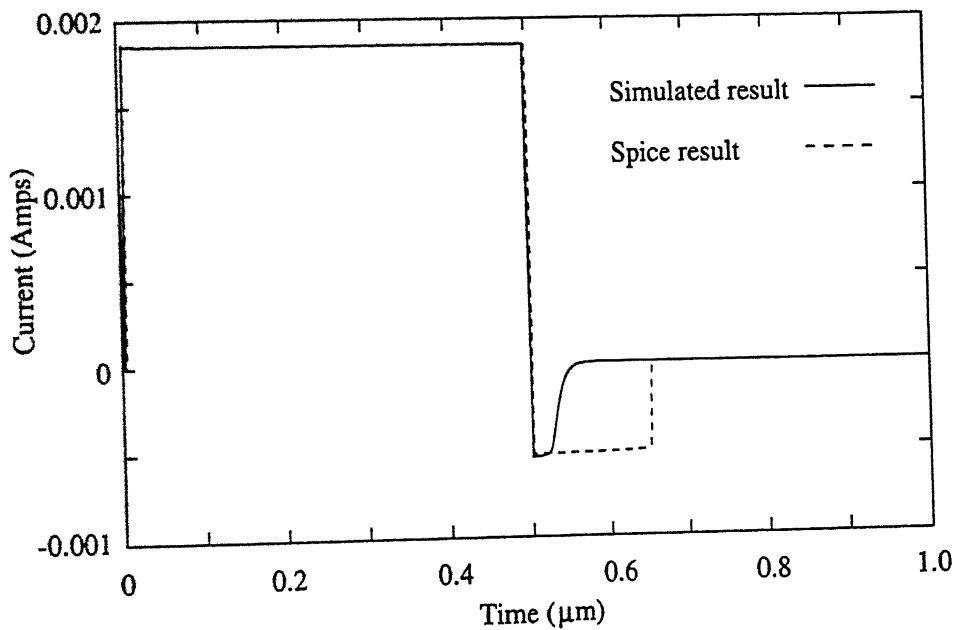


Figure 3.33: Diode current vs time.

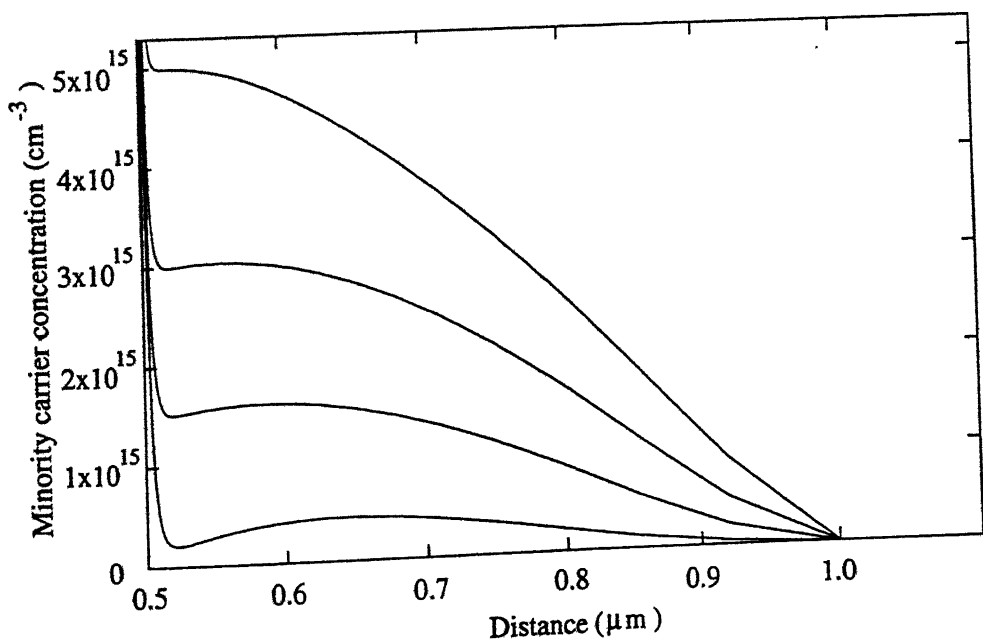


Figure 3.34: Minority carrier concentration vs distance for a short base diode after the negative edge of the voltage step.

## Chapter 4

# Conclusion and scope for future work

In the present work, numerical solution of basic semiconductor equations under transient conditions is presented. Carrier concentrations and potential in the interior of the device for time dependent current or voltage excitation are shown. This analysis allows a thorough understanding of the basic time dependent phenomena governing the physical behaviour of the semiconductor device under typical external excitations.

We have found good agreement between our simulation results and theory with respect to storage delay time. On the other hand, analytical expression was found to underestimate the fall time delay substantially. SPICE simulation gives very large storage delay time while it does not give any fall time delay. The steady state solution and the transient solution represent a powerful tool of investigation in areas of computer aided device modelling, in particular the analysis of devices under switching conditions.

In the present work, complications such as Auger recombination, nonuniform doping density, etc., are not considered because we wanted to compare our results with the analytical expressions which are also derived under simple assumptions. To come close to the real diode more extensive studies are required so that all the effects are considered. As the numerical simulation results are more accurate, improved models for practical diodes can be suggested.

## References

1. H.K Gummel, "A self consistent scheme for one dimensional steady state transistor calculations" , IEEE Trans. Electron Devices, Vol. ED-11, pp. 455-465 (1964)
2. A. De Mari, "An Accurate steady state one dimensional solution of pn-junction", Solid State Electron, Vol.11, pp.33-58 (1968)
3. D.L Scharfetter and H.K Gummel, "Large signal analysis of a silicon read diode oscillator", IEEE Trans. on Electron Devices, Vol. ED-16, pp.64-77 (1969)
4. Siegfried Selberherr, "*Analysis and simulation of semiconductor devices*", Springer verlag, New York, 1984.
5. P. Ravi kumar, "*Validation of text book model for capacitance of a forward biased pn junction*", M.Tech Thesis Dept of Electrical Engg. IIT Kanpur, 1999.
6. R. Raghuramam "*Computer simulation of electronic circuits*". Wiley Eastern Limited, 1991.
7. A. De. Mari, "An accurate one dimensional solution of the pn junction diode

- under arbitrary transient conditions", Solid state electronics, Vol.11, pp.1021-1053. (1968).
8. M.S Tyagi, "*Introduction to semiconductor materials and devices*", John wiley and sons, 1991.
  9. W. H. Ko, "The reverse transient behaviour of semiconductor junction diodes", IRE Trans. on Electron Devices, Vol. ED-8, pp.123-131, March, (1961)
  10. S. M. Sze, "*Physics of semiconductor devices*", John Wiley, New York, 1981.
  11. M. H. Rashid, "*SPICE for circuits and electronics using PSPICE*", Printice Hall of India. Pvt. Limited, New Delhi, 1995

1

Da

## Da

book is

[illegible]

A127973

TH

EE/1999/M

Sh230

A127973